Ultrastructure of Selenidium pendula, the Type Species of Archigregarines, and Phylogenetic Relations to Other Marine Apicomplexa

Joseph Schrével, Andrea Valigurová, Gérard Prensier, Aurélie Chambouvet, Isabelle Florent, Laure Guillou

ORIGINAL PAPER

Ultrastructure of *Selenidium pendula,* the Type Species of Archigregarines, and Phylogenetic Relations to Other Marine Apicomplexa

Joseph Schrével[a,1], Andrea Valigurová[b], Gérard Prensier[c,2], Aurélie Chambouvet[d], Isabelle Florent[a], and Laure Guillou[e]

[a]Unité Molécules de Communication et Adaptation des Microorganismes, (MCAM, UMR 7245), Muséum National Histoire Naturelle, Sorbonne Universités, CNRS, CP 52, 57 Rue Cuvier, 75005 Paris, France

[b]Department of Botany and Zoology, Faculty of Science, Masaryk University, Kotlářská 2, 611 37 Brno, Czech Republic

[c]Cell Biology and Electron Microscopy Laboratory, François Rabelais University, 10 Boulevard Tonnellé, BP 3223, 37032 Tours Cedex, France

[d]Laboratoire des Sciences de l'Environnement Marin (LEMAR), UMR6539 UBO/CNRS/IRD/IFREMER, Institut Universitaire Européen de la Mer (IUEM), Technopole Brest Iroise, 29280 Plouzané, France

[e]Sorbonne Universités, Université Pierre et Marie Curie - Paris 6, CNRS, UMR 7144, Station Biologique de Roscoff, Place Georges Teissier, CS90074, 29688 Roscoff cedex, France

Submitted February 3, 2016; Accepted June 12, 2016

Monitoring Editor : Frank Seeber

Running title: *Selenidium pendula*: Ultrastructure and Phylogeny

[1]Corresponding author; fax +33 1 40 79 34 99

e-mail schrevel@mnhn.fr (J. Schrével).

[2]This work is dedicated to the memory of Brigitte Arbeille-Brassart

Archigregarines, an early branching lineage within Apicomplexa, are a poorly-known group of invertebrate parasites. By their phylogenetic position, archigregarines are an important lineage to understand the functional transition that occurred between free-living flagellated predators to obligatory parasites in Apicomplexa. In this study, we provide new ultrastructural data and phylogenies based on SSU rDNA sequences using the type species of archigregarines, the Selenidiidae *Selenidium pendula* Giard, 1884. We describe for the first time the syzygy and early gamogony at the ultrastructural level, revealing a characteristic nuclear multiplication with centrocones, cryptomitosis, filamentous network of chromatin, a cyst wall secretion and a 9+0 flagellar axoneme of the male gamete. *S. pendula* belongs to a monophyletic lineage that includes several other related species, all infecting Sedentaria Polychaeta (Spionidae, Sabellaridae, Sabellidae and Cirratulidae). All of these *Selenidium* species exhibit similar biological characters: a cell cortex with the plasma membrane - inner membrane complex - subpellicular microtubule sets, an apical complex with the conoid, numerous rhoptries and micronemes, a myzocytosis with large food vacuoles, a nuclear multiplication during syzygy and young gamonts. Two other distantly related *Selenidium*-like lineages infect Terebellidae and Sipunculida, underlying the ability of archigregarines to parasite a wide range of marine hosts.

Key words: Archigregarines; Apicomplexa; *Selenidium pendula*; ultrastructure; phylogeny; sporozoite.

Introduction

Apicomplexa, a large subgroup of the Alveolata, are unicellular parasites infecting a wide range of invertebrate and vertebrate hosts. Most known Apicomplexa belong to Coccidia and Haemosporidia and are involved in human and veterinary diseases (malaria, toxoplasmosis, coccidiosis, babesiosis, piroplasmosis). However, a very large group of the early branching Apicomplexa, the gregarines, is comparatively poorly known. Most of the gregarines infect invertebrate hosts and usually do not have deleterious effects on their

hosts (Desportes and Schrével 2013). The number of Apicomplexa species is estimated to be ~2,000-6,000, however the ability of gregarines to infect a wide range of insects could significally enhance this estimation to several thousand or more than one million (e.g., the Coleoptera (beetles) class corresponds to about 40% of the insect biodiversity with an expected species number around 1 to 2 million) (Schrével and Desportes 2013).

All apicomplexan species are characterized by an infective life stage, the so-called zoite, a polarized cell with an original apical complex. This apical complex is an assembly of specific organelles including club-shaped rhoptries, filament-like micronemes, dense granules and apical polar rings. In Apicomplexa, the presence of a conoid in the apex of the zoite, observed in coccidia and gregarines, defines the Conoidasida Levine, 1988. In contrast, no conoid is observed in Haemosporidia and Piroplasmida designated Aconoidasida by Mehlhorn et al. (1980). Except gregarines and some other taxa developing in epicellular localization, such as cryptosporidia, most Apicomplexa have an intracellular development in their host cells and there, the apical organelles as well as the conoid, play an essential role in cell invasion processes through sophisticated cascades of molecular interactions (Boothroyd and Dubremetz 2008; Bradley et al. 2005; Santos et al. 2009). In Apicomplexa displaying an intracellular life style, the cycle usually occurs in two hosts, the sexual phase being performed in the definitive host while asexual phases occur in one or several intermediate hosts. Gametogenesis, as observed in Coccidia or Haemosporidia, exhibits a clear anisogamy with production of small flagellated male gametes (microgametes) and large non-flagellated female gametes (macrogametes). After fertilization, the sporogony produces sporozoites in the definitive hosts while asexual schizogny or merogony, producing merozoites, is realized in intermediate hosts. In contrast, most gregarines exhibit an extracellular development and their entire life cycle usually occurs within a single host. Their zoites transform into large vegetative cells, the trophozoites, with an extraordinary diversity in their morphologies and behaviours. In addition to this extracellular development, gregarines share a unique sexual phase. The sexual association between two gamonts, named syzygy, produces a cyst where the gametogenesis differentiates a large and equal number of male and female gametes; at this stage, this cyst is called a gametocyst. Then, fertilization and sporogenesis take place within the cyst yielding the final stages with the sporocysts usually containing each 8 sporozoites. These sporocysts can survive for a long period generally waiting for their ingestion by their specific hosts. Gregarine biochemistry and physiology are still poorly documented. Studies of their zoite apical apparatus as well as of the variation of their

cytoskeleton and microtubule organizing centers (MTOCs), with unique organization as the 6+0 or 3+0 flagellar axonemes described for some male gametes (Prensier et al. 1980; Schrével and Besse 1975), contributed, however, to a more general understanding of many biological aspects of Apicomplexa including pathogenic species.

Among Apicomplexa, there is a consensus on the stem group of archigregarines commonly found in Polychaeta, Sipunculida and some Hemichordata. These marine gregarines represent the earliest diverging lineage of Apicomplexa (Leander 2007a; Schrével 1971b). The type species of archigregarines is *Selenidium pendula* Giard 1884 and its life cycle was established during the second part of the 20th century (Schrével 1966, 1970). Beside this type species, a long series of contributions have been performed on other *Selenidium* and related species at the cytological (Brasil 1907, Caullery and Mesnil 1899, 2000, Ray 1930, Reed 1933) and ultrastructural (Leander 2006, 2007b; Macgregor and Thomasson 1965; Schrével 1968, 1970, 1971a; Simdyanov and Kuvardina 2007, Vivier and Schrével 1964, 1966) levels and more recently also at the molecular level through the analysis of SSU rDNA sequences (Leander et al. 2003; Leander 2006, 2007b; Rueckert and Leander 2009; Wakeman and Leander 2012, 2013; Wakeman et al. 2014). Most of these studies focused on the trophozoite stages with few descriptions on nutrition modalities (Schrével 1968; Simdyanov and Kuvardina 2007). Additionally, these studies highlighted several incongruities among Selenidiidae at the molecular level that could not be elucidated in absence of the type species of the family. Here, we report on the cell organization of the *Selenidium pendula* trophozoite with a special attention to the conoid, the abundance of rhoptries and micronemes, and we provide the first ultrastructural description of the syzygy (pairing stage), the early gamogony with the cryptomitosis and the secretion of the cyst walls. We also provide the first phylogenetic analysis of the SSU rDNA gene sequences encompassing the type species of archigregarines *S. pendula*. Molecular phylogenetic analyses revealed three lineages within archigregarines, *S. pendula* belonging to the Selenidiidae that includes parasites of Spionidae, Sabellidae, and Sabellariidae, all polychaete annelids, as well as two Selenidiidae–like lineages, parasites of hosts belonging to Terebellidae and Sipunculida, respectively.

Results

The Trophozoite of *Selenidium pendula*

The mature *S. pendula* trophozoite is a crescent-shaped cell of about 150 µm in length with a circular cross section of about 35 µm in diameter. The cell surface exhibits about 30 striations in phase contrast light microscopy as well as in scanning electron microscopy (SEM), appearing as a series of longitudinal bulges of about 2.5-3 µm in width separated by grooves (Fig. 1A). The trophozoite is inserted into the intestinal epithelium of the *Scolelepis squamata* polychaete worm by a special apical apparatus called the mucron (Figs 1B, 2A-C). In transmission electron microscopy (TEM), a tropism for host cells rich in granules can be observed (Fig. 1B). The mucron of *S. pendula* corresponds to the attachment apparatus anchoring the parasite to the host epithelial cell. In SEM, the mucron appears as a regular mammiliform area without bulges and grooves (Fig. 2A). After detachment of the trophozoite, the trace of the mucron in the host cell is very regular with sometimes a small hole in a subcentral position (Fig. 2B).

A series of short microvilli is seen at the periphery of the epithelial cells (Fig. 2B). All around the trophozoite attachment, numerous long ciliary structures of the host epithelium are observed (Figs 1A, 2B).

Asexual schizogony in *S. pendula* could be an explanation to the exceptional clotting of trophozoites, with thousands and thousands of cells that obstruct the intestinal lumen of some *Scolelepis squamata* hosts. In vivo, trophozoites are dispersed along the host intestine, except for the first thirty segments. The distinction between these two intestinal regions is facilitated by the yellow color of the first segments versus the green color of the posterior region. Motility of the *S. pendula* trophozoites is clearly of pendular type, as proposed by Giard (1884) for the species diagnosis, and the stroboscopic records show regular pendular beats with a period of about 0.2 second (Golstein and Schrével 1982).

In TEM cross sections, the bulges of *S. pendula* exhibit a characteristic ultrastructure described for the first time in *Selenidium hollandei* (Vivier and Schrével 1964). The plasma membrane is underlain by a regular flat vesicle designated as the inner membrane complex (imc) while a very slight cell coat covers the cell surface. Under these three cortical membranes, a regular set of longitudinal subpellicular microtubules and some other dispersed microtubules within the cortical cytoplasm are seen below the bulges but not in the area of the grooves (Fig. 3B-C). In TEM cross sections, each subpellicular microtubule of *S. pendula* is surrounded by an electron-lucent sheath (Fig. 3C) as observed in *S. hollandei* (Vivier and Schrével 1964), *Platyproteum (Selenidium) vivax* (Leander

2006), *Selenidium serpulae* (Leander 2007) and *Selenidium terebellae* (Wakeman et al. 2013). Abundant mitochondria are present under the subpellicular network of the bulges.

Different ectoplasmic structures along the grooves are observed with lamellar elements, dense material structures that crossed the imc and are in contact with the plasma membrane (Fig. 3B, D-F). Under SEM, series of holes are observed in the grooves with an irregular distribution and distances ranging from 0.3-0.4 µm to 0.8-0.9 µm (Fig. 3A). Such a distribution seems to correspond to the opening sites of the above-mentioned ectoplasmic structures and their density might indicate a role that was previously underestimated.

Interestingly, the longitudinal microtubular bundles, abundantly distributed beneath the cortex in the trophozoite apical part corresponding to the mucron, could represent the biogenesis site of the longitudinal networks of the subpellicular microtubules (Fig. 2D).

Conoid and Myzocytosis

The conoid of *S. pendula* is a truncated cone of about 225 nm height, with apical and distal diameters about 260 nm and 1 µm respectively (Fig. 4A-C). In TEM cross sections, the diameter of filaments is about 23-32 nm; 9 sections are well identified in one side of the conoid, while only an opaque layer can be observed on the other side due to their spiral organization (Fig. 4B-C). This structure is quite similar to the well-described conoid of *Toxoplasma gondii* (Hu et al. 2002, 2006) but the apical polar ring is not present in the distal part of *S. pendula* mucron and the preconoidal rings are not clearly identified in its apical part but a dilatation of the imc and the ends of the subpellicular microtubules are unambiguously demonstrated (Fig. 4A, C, white arrows). This imc dilatation could correspond to a site of a Microtubule Organizing Center (MTOC) able to generate the subpellicular microtubules since abundant bundles are found in the anterior area of the trophozoite (Fig. 2D). In few TEM cross sections, dense structures corresponding to the neck of the rhoptries are observed inside the conoid (Fig. 2C).

Myzocytosis, the predatory mode of nutrition characteristic of archigregarines, is clearly illustrated in *S. pendula* with food vacuoles inserted inside the conoid (Figs. 2C, 4A-B). In the axis of the mucron, one or several clear food vacuoles, likely formed via the conoid, are present (Fig. 2C). These food vacuoles are surrounded by many rhoptries and micronemes, two apical organelles characteristic of zoites (Figs 1B, 2C). As shown by the continuity of the food vacuole membrane up to its contact with the host epithelial cell, an evagination process through the apex of the conoid has occurred, allowing the parasite to suck out the nutriments from the host. This myzocytosis process starts at the top of the

conoid (Fig. 4A). The food vacuoles are large, reaching sometimes up to 7 µm, and several additional food vacuoles of about 2 or 3 µm are observed in the axis of the trophozoite (Figs 2C, 5A-B). The lumen of the food vacuoles has a low electron-dense aspect with some vesicles and the membrane of the food vacuole exhibits a very irregular border with numerous digitations.

Vital staining with low concentrations of neutral red (1 $^{0}/_{00}$) allowed to visualize large vacuoles of about 4x2 µm located in the apex of the *S. pendula* trophozoite with several small vesicles (data not shown). This observation is in agreement with a fragmentation of the initial food vacuole into numerous vacuoles present in the anterior part of the trophozoite (Fig. 5A).

Rhoptries, Micronemes, and Intrareticular Granules in Trophozoites

In addition to the conoid, the apical end of *S. pendula* trophozoites exhibits about 8-10 rhoptries corresponding to the long, electron-dense club-shaped, tubular or saccular organelles. They appear in the trophozoite as cylindrical organelles reaching up to 6 µm in length, with a diameter of 0.3-0.4 µm in the basal bulbous. At the apex, a rhoptry neck could be observed. The rhoptry orientation usually follows the direction of the conoid. In some cases, the rhoptry neck penetrates the conoid (Fig. 2C).

The rough endoplasmic reticulum (RER) and the Golgi apparatus of *S. pendula* show an original association between the swollen cisternae containing numerous intrareticular granules of about 0.5-1 µm and the first saccule of the cis-region of the Golgi apparatus (Fig. 6D). Similar associations are observed in *S. hollandei* (Vivier and Schrével 1966) but not in Selenidiidae species parasitizing Cirratulidae (Schrével 1971), Serpulidae (Leander 2006), Terebellidae (Wakeman et al. 2014) or Sipunculida (Simdyanov and Kuvardina 2007, Leander 2007). Some micrographs show an accumulation of numerous micronemes close to the nuclear envelope (Fig. 7D) or to the Golgi apparatus (Fig. 6C) with annular sections likely corresponding to the neck of micronemes (Fig. 6B). The relation of these RER-Golgi apparatus to the biogenesis of the rhoptries and/or the micronemes is not clear, since numerous micronemes are mixed with large rhoptries (Fig. 6A).

Nucleus and the Perinuclear Cytoplasm

The ovoid nucleus of the *S. pendula* trophozoite is characterized by the presence of a large spherical nucleolus of about 4-5 µm in diameter (Fig. 7A). No accumulation of chromatin is observed in the nucleoplasm and the nuclear envelope lacks the nuclear lamina as observed in *S. hollandei* (Schrével 1971a; Vivier 1967). The nuclear envelope, typically comprising two membranes, is rich in nuclear pores (about 5 per µm) regularly distributed all over the entire nuclear surface (Fig. 7C). In tangential sections, the pores appear as rings of about 100-110 nm in their largest diameter with the presence of a central particle of about 10 nm in diameter (Fig. 7C).

The periphery of the nucleus exhibits a special cytoplasmic area comprising a regular, 0.5 µm thick fibrillar zone, lacking any organelle, and surrounding the nucleus in a distance of 1.5-2 µm from the nuclear envelope (Fig. 7A-B, E). This fibrillar zone corresponds to the axial ducts described in living cells (Schrével 1970).

Apicoplast-like Organelles

In the trophozoite of *S. pendula*, organelles with four membranes are frequently observed (Fig. 5C) and they appear morphologically similar to the apicoplast of *Toxoplasma* and *Plasmodium* (Lim and McFadden 2010) with some dense structures (Fig. 5D) or in contact with multilamellar organelle (Fig. 5E).

Nuclear Multiplication During the Syzygy and Young Gamonts

The sexual phase of the *S. pendula* life cycle starts with the syzygy, characterized by the pairing of two haploid trophozoites, now called gamonts: one male and one female. During the young syzygy stage of *S. pendula,* the two gamonts are linked by their posterior parts, while their pendular motility continues with waves starting from the apex to the posterior end (Schrével, 1970).

In TEM, each gamont exhibits a similar intracellular organization with a nucleus of about 20 µm in diameter containing a spherical nucleolus of about 5 µm in diameter (Supplementary data 1). In each nucleolus, several clear areas are observed with sizes varying from 0.3 to 1 µm in diameter (Supplementary data 1, arrows). The cell surface and the cytoplasm of the two gamonts also exhibit a similar organization (Supplementary data 1).

A clear characteristic of archigregarines belonging to the family Selenidiidae is the early nuclear multiplication within the two gamonts at the site corresponding to the initial trophozoite nucleus that occurs before the encystment of the gamonts. The localization of

the nuclei at the initial site of the trophozoite nucleus is clearly shown by the DAPI staining highlighting the DNA-containing structures (Fig. 8A-B). Bright spots are observed inside spherical structures, each of them corresponding to a nucleus. In about two hours, the pendular motility of each gamont is progressively reduced and cyst formation occurs with a widening of the nuclear zone in the gamont's median plane (Fig. 8A-B). In TEM, the concentration of the nuclei at this stage is not easy to observe due to the relatively high rate of this process. In favourable cross sections, the nuclei are observed in the central area of the gamont and before the secretion of the cyst wall. Each spherical nucleus is about 5 µm in diameter (Fig. 8C). From this central site, the nuclei migrate to the periphery of each gamont while the cyst wall is forming (Fig. 8D). In many nuclei of the gamonts, centrocones and other stages of cryptomitosis were detected.

Centrocones and Cryptomitosis in Gamonts

The mitosis in *S. pendula* gamonts is a closed-mitosis, also called cryptomitosis, with the persistence of the nuclear envelope as observed in all Apicomplexa (Francia and Striepen 2014). All the nuclei of the *S. pendula* gamonts are spherical with a diameter of about 5 µm and many are associated to a cupule with microtubules radiating from the Microtubule Organizing Center (MTOC) in order to form half-spindles (Fig. 9A-B). The chromatin is localized all around the internal face of the nuclear envelope as shown in TEM images (Fig. 9A-B). This chromatin forms an electron dense filamentous network with spotty dark nodes and in some cases, an important dense accumulation is observed inside the nucleoplasm (Fig. 9A). This dense accumulation of at least 1 µm could correspond to the bright spots visualized by the DAPI-staining (Fig. 8B). The distribution of chromatin in *S. pendula* nucleus appears as a continuous filamentous network quite similar to the model of Apicomplexa cryptomitosis proposed by Francia and Striepen (2014).

In *S. pendula* gamonts, many nuclei exhibit a centrocone resulting probably from the high rate of nuclear divisions since the chronology from the syzygy to the encystment of the gamonts represents only 2-3 hours (Schrével 1970). The centrocone depends upon the MTOC that appears as an electron dense annular structure of about 200 nm in diameter. From the MTOC, microtubules radiate and form a half-spindle that pushes the nuclear envelope without penetration in the nucleus (Fig. 9A). The resulting cupule exhibits an outer diameter of about 1.6-1.9 µm and the distance from the MTOC to the inner border of the cupule is about 1.4-1.6 µm. This typical centrocone can duplicate and the second centrocone migrates to the opposite direction of the initial cupule (Fig. 9B). Micrographs

with two centrocones are rather rare and an intranuclear spindle was not observed most likely due to the high rate of the progamic nuclear division in *S. pendula.*

As the progamic nuclei migrate from the central part of the gamont to the periphery, the cryptomitosis continues after this migration, since the duplication of the centrocones is observed in the border of the cyst where the wall is secreted.

Modifications of the Gamont Cell Surface and Secretion of the Gametocyst Wall

When the gametocyst wall is forming, the cortical membranes of each gamont are strongly modified (Fig. 10A-C). The plasma membrane is always present but the imc is disorganized with a series of folds and clear dissociation from the plasma membrane (Fig. 10B-C). In TEM, the gametocyst wall exhibits two major layers, a homogeneous internal layer of about 500-700 nm in thickness and a fuzzy external layer with long filaments reaching about 300 nm. The total thickness of the gametocyst wall at the beginning of gamogony is about 1 µm. The secretion of this wall is the result of two types of vesicles, one with rather electron dense components (vesicle 1) and the second with a network of very spotty filaments (Fig. 10A). The mechanism of discharge of these two types of vesicles was not clearly observed. As the gametocyst wall formation occurs only two hours after the early syzygy step, the secretion is probably the result of accumulations of numerous intrareticular granules in the cisterns of the rough reticulum endoplasm that represent storage material for this process (Fig. 6D). However, a potential dual function of the RER-Golgi apparatus for both the formation of rhoptries and micronemes and the storage of material for gametocyst formation needs further investigations (Fig. 6A).

The Gametocyst and the Sporocyst Walls

The gametogenesis is a fast process in *S. pendula,* lasting about one hour (Schrével 1970). After the series of progamic nuclear divisions yielding syncytium nuclei in the same gametocyst, cellularization occurs, producing flagellated male gametes and female gametes without flagellum. In TEM, the gametocyst wall is more compact with dense layers (Fig. 11A-B). The fuzzy coat observed at the beginning of the gamogony is now very irregular in width and the internal homogenous layers are more electron dense (Fig. 11A). In some cases the internal layers show a regular opaque layer of 0.3 µm and an irregular homogenous layer with a lower electron density (Fig. 11A).

In cross sections, the flagellar axoneme of the male gamete of *S. pendula* exhibits a 9+0 pattern (Fig. 11B2). After fecundation, the life cycle moves into the sporogony phase with the formation of sporocysts corresponding to the evolution of the zygotes toward the sporozoite formation inside each sporocyst. A new secretion process occurs around this sporocyst (Fig. 11C). The thickness of the sporocyst wall is about 0.1 μm with small thin spine-like digitations of about 0.2 μm (Fig. 11C).

Molecular Phylogenetic Analyses of the SSU rDNA Sequence

Type species are important to build solid bridges between molecular phylogenies and taxonomy. A phylogenetic tree was constructed using 115 sequences including nine novel small subunit (SSU) rDNA sequences (two sequences from *S. pendula*, the type species for Selenidiidae, one from *S. hollandei*, one from *Lecudina pellucida*, the type species for Lecudinidae, and 5 from *L. tuzetae*, all specimen isolated from host organisms collected in the Roscoff area, France) and 106 previously published ones available from public databases, taking into account all available data for archigregarine species (Table 1). Sequences known to produce extreme long branches in SSU rDNA-based phylogenies, such as those of the gregarines *Trichotokara* spp. *and Pyxinia robusta,* were excluded from this analysis. Globally, the Maximum Likelihood and the Bayesian tree topologies were congruent (Fig. 12) and in good agreement with recently published phylogenies (Wakeman and Leander 2013; Wakeman et al. 2014). The two early lineages emerging among Apicomplexa were from marine gregarines with archigregarines and eugregarines. Interestingly the phylogenetic position of the type species *Lecudina pellucida* (Fig. 12) fell within the Lecudinidae, with a good support with lecudinids of tunicates represented by the *Lankesteria* genus. In the terrestrial gregarines, the *Gregarina* lineage belongs to rather old insects such as Coleoptera, Blattaria, and Orthoptera, in contrast to the *Ascogregarina* lineage that infects more recent insects according to the most recent knowledge on insect evolution (Misof et al. 2014).

An analysis of the SSU rDNA sequences clearly demonstrated the paraphyly of Selenidiidae, which are split into three major groups (Fig. 13, Supplementary Material 2-4). The type species *Selenidium pendula* is closely related to *Selenidium boccardiella* (Wakeman and Leander 2013). These two gregarines infect members of the Spionidae family of Polychaeta. Similarly, *S. hollandei* is closely related to *S. neosabellariae* and *S. identhyrsae* (Wakeman and Leander 2013), these three species being parasites of hosts

belonging to Sabellariidae. Parasites infecting Spionidae and Sabellariidae diverged from 3.4 to 13.7 % from each other (sequence identity, Supplementary Material 2, 3).

Selenidium parasites of Terebellidae group form a second divergent lineage with a wider global divergence with true Selenidiidae of 25.8-28.2 %, (Supplementary Material 2, 3). Finally, all Selenidiidae described in *Phascolosoma* formed a third group which is the most divergent (26.3 - 28.8 % of divergence with the two precedent groups, Supplementary Material 2, 3).

Discussion

Selenidium spp. and archigregarines

Since 2003, the morphology of some trophozoites of Selenidiidae and related archigregarines was investigated using SEM and more than 25 SSU rDNA sequences were deposited in the GenBank/EMBL/DDBJ databases (Leander 2003, 2007; Leander et al. 2003; Rueckert and Leander 2009; Wakeman and Leander 2012, 2013; Wakeman et al. 2014). However, data on sexual stages (gamogony and sporogony) were missing. By combining electron microscopic descriptions with phylogenies using SSU rDNA sequence data, new *Selenidium* species have been proposed such as *S. pisinnus* Rueckert and Leander, 2009, *S. boccardiella* Wakeman and Leander, 2012, *S. idanthyrsae* Wakeman and Leander, 2012, *S. neosabellariae* Wakeman and Leander, 2013, *S. sensimae* Wakeman and Leander, 2013 and *S. melongena* Wakeman et al., 2014. A new genus *Platyproteum* (Rueckert and Leander 2009) was erected to replace the former species *Selenidium vivax* (Gunderson and Small 1986). A new enigmatic genus related to archigregarines was also proposed as *Veloxidium* (Wakeman and Leander 2013). In their discussion, Leander and co-workers produced a comparative table with morphological data of all Selenidiidae described in the last century (Ray 1930; Schrével 1970, 1971). Few mistakes within Selenidiidae were reported in this table (table 2 in Wakeman and Leander 2012) as for example the mention of *S. spionis,* presented as a parasite of *Polyrabdina spionis*. *Polyrhabdina spionis* is in fact a lecudinid gregarine and the host of *S. spionis* is the polychaete *Scolelepis fuliginosa* (Claparède, 1870) now called *Malacoceros fuliginosus* (Claparède, 1870) (Schrével and Desportes, 2013). However, the SSU rDNA sequences analysis of *S. spionis* revealed lineages inside archigregarines and Leander and co-workers underlined the importance of future work on additional *Selenidium*-like gregarines

especially the type species *S. pendula* (Wakeman et al 2014). This current work on the type species *S. pendula* Giard, 1884 and on *S. hollandei* Vivier and Schrével, 1966 therefore enlighten with less ambiguities parts of the evolutionary history of archigregarines.

The SSU rDNA sequence phylogeny trees with the different SSU rDNA sequences of archigregarines (Table 1), show three clearly delimited lineages among Selenidiidae (Figs 12-13, Supplementary Material 3, 4). A major group corresponds to the true-*Selenidium* lineage, for which sexual stages (syzygy to sporocyst) have been described. Its members are parasites of Sedentaria polychaetes, such as *S. pendula* that infects the Spionidae family, *S. hollandei* infecting Sabellariidae and *Selenidium* cf. *meslini* infecting Sabellidae. These true-*Selenidium* share common important features, such as a nuclear multiplication during the syzygy, the gamogony and the sporocysts with usually four sporozoites. Many archigregarines have developed atypical variations in their cell morphology and their motility from pendular to rolling type, with subpellicular microtubule sets under the inner membrane complex (imc), but without the gliding type observed in eugregarines. Trophozoites of true-*Selenidium* exhibit a three-membrane cortex where the imc forms a complete envelope underlying the plasma membrane, with sets of longitudinal subpellicular microtubules running under the large folds designated as bulges (Schrével 1970a, 1971a; Schrével et al. 2013; Vivier and Schrével 1964). The grooves correspond to the striations well described this last century by light microscopic (Brasil 1907; Ray 1930; Schrével 1970). The cytoplasm beneath the grooves is devoid of microtubules but exhibits micropores and residual membranous organelles in connection with the imc (Schrével et al. 2013; Vivier and Schrével 1964). These parasites feed by myzocytosis using the conoid located at the apex of the trophozoite (Schrével 1968, Simdyanov and Kuvardina 2007, this work).

In this true-*Selenidium* lineage, the sexual stage starts by the syzygy where the formation of progametic nuclei is observed inside the gamont nucleus before encystment. This observation in the type species *S. pendula* (Fig. 8) is the confirmation of histological previous descriptions by Caullery and Mesnil (1900), Ray (1930), Reed (1933), Tuzet and Ormières (1958) and in vivo observations by Schrével (1970). This gamogony is quite different from all other eugregarines where the first gamogony division starts inside the cyst and is followed by successive series of nuclear divisions called progamic mitoses without cytokinesis such as in *Lecudina tuzetae* (Kuriyama et al. 2005). So, the *Lecudina* type gamogony produces a syncytium until the cellularization process yielding the gametes. Another clear difference concerns the degree of condensation of the chromatin with a

continuous filamentous network attached to the nuclear envelope all around the nucleus in *S. pendula* cryptomitosis. Chromosome condensation does not seem to occur in *S. pendula* in contrast to cryptomitosis of *L. tuzetae* (Kuriyama et al. 2005) and *Grebnickiella gracilis* (Moblon-Noblot 1980). Sporogony then leads to spherical sporocysts that differentiate usually into four sporozoites per sporocyst (Ray 1930; Schrével 1970).

Other *Selenidium*-like species infecting sipunculids and Terebellidae are only known through their trophozoites and their localization within hosts (Leander 2006; Wakeman et al. 2014). The intestinal trophozoite of *S. terebellae* Ray 1930 exhibits large bulges but differences with the true-*Selenidium* have been observed. As an example, a regular layer of about 30-33 nm in thickness (Supplementary Material 5 and Wakeman et al. 2014) similar to the internal lamina of eugregarines (Schrével et al. 1983) or to some euglenoid cortex (Mignot 1966) is attached to the imc. Numerous sets of longitudinal subpellicular microtubules are immediately under this regular dense layer and many residual membranous organelles are highly concentrated under the imc of the grooves (Supplementary Material 5). *S. melongena* trophozoites were described in the same host as *S. terebellae*, but inside the coelom, an unusual localization for archigregarines (Wakeman et al. 2014). The cortex of *S. melongena* exhibits 30-40 epicytic folds helically arranged along the axis of the cell. Surprisingly, although the subpellicular sets of microtubules were not observed in TEM, a strong fluorescent labelling of alpha-tubulin was detected below the helical folds. *S. melongena* are non-motile without pendular or rolling motility nor gliding. According to Wakeman et al. (2014), such atypical cell organization of *S. melongena* trophozoites seems to be closer to lecudinids than to Selenidiidae. These original observations as well as the lack of description of syzygy and sporocysts require future work, especially to explain the way by which *S. melongena* can infect its host.

The third *Selenidium*-like lineage described here corresponds to a group of intestinal parasites of Sipunculida. These parasites are mainly known from SEM and TEM observations on *Selenidium vivax* trophozoites (Leander 2006). Renaming of *S. vivax* as *Platyproteum vivax* was supported by archigregarine flat shape when observed under TEM with important sets of longitudinal subpellicular microtubules and numerous mitochondria probably in relation to the very active plasticity of *S. vivax* (Rueckert and Leander 2009). This cellular organization appears similar to that of *S. hollandei* (Schrével 1970). Here also, descriptions of the syzygy with their characteristic progametic nuclei as well as the sporocysts require clarifications. This point is also important for *Filipodium* trophozoites

where numerous microvilli from 1.6-10 µm long and about 0.15 µm in diameter were clearly described in TEM (Hoshide and Todd 1996).

All archigregarines are intestinal parasites of Annelida belonging to the clade Sedentaria except one *Selenidium metchnikovi* reported in Hemichordata (Léger and Duboscq 1917). In contrast, many lecudinids are intestinal parasites of the clade Errantia from Annelida (Schrével and Desportes 2013). This separation between archigregarines and marine lecudinid eugregarines is probably related to the different modes of living of their hosts. For instance, lecudinids are adapted to the errant and predatory life of Errantia while archigregarines are adapted to sedentary life of Sedentaria with microphage species living below stones, or as tube builders or ingesting sediment as the representatives of the family Spionidae or surface deposit feeders with head appendages (Sabellidae, Sabellariidae). Evolutionary history of Annelida is still poorly understood as the classic morphological cladistic analysis with a monophyletic Polychaeta (Rouse and Fauchald 1997) was challenged in the light of the recent molecular evidences. Today, Polychaeta are inferred to be paraphyletic with the inclusion of the Clitella (earthworms) and the non-segmented taxa Echiura and Sipunculida (Struck et al. 2011). Complexity of the phylogeny of *Selenidium* species may reflect the one of their hosts. The true-*Selenidium* lineage within the Selenidiidae family likely forms the core of archigregarines while the two other distant lineages infecting respectively the Sipunculids and Terebellids orders, could be considered as related *Selenidium*-like lineages. These results, deduced from molecular phylogeny analyses need to be confirmed at the biological and cellular levels but are crucial since they open new trends in evolutionary history among Apicomplexa.

The enigmatic *Veloxidium leptosynaptae,* initially placed within archigregarines after phylogenetic analyses (Wakeman and Leander 2012) was later included within lecudinids and urosporids (Wakeman et al. 2014). In our phylogenetic studies, it also groups with lecudinids and urosporids with strong supports (Fig. 12).

Apicoplasts, Conoid, MTOC and Rhoptries are Major Cell Structures in the Evolution of Apicomplexa

Gregarines represent interesting models to investigate the evolution from free-living flagellated alveolates status, likely photosynthetic, to obligatory parasites among Apicomplexa.

In archigregarines, the presence of an apicoplast remains an open question. Presence of a functional plastid is reported in *Chromera*, a free-living photosynthetic relative to

Apicomplexa (Lim and McFadden 2010). The apicoplast, a non-photosynthetic plastid of red algae origin, is well documented in some Apicomplexa species such as *Plasmodium*, *Toxoplasma*, *Eimeria*, *Babesia*, *Theileria*. This relict plastid is limited by four membranes indicating its secondary endosymbiont origin. In the eugregarine *Gregarina niphandrodes*, the apicoplast seems to be absent (Toso and Omoto 2007). Here in *S. pendula*, apicoplast-like organelles are regularly observed in trophozoites at the ultrastructural level. Interestingly Ray (1930) reported the visualization of a dark spot stained with Heidenhain's haematoxylin, associated to each merozoite nucleus in *S. mesnili* parasitizing the polychaete *Myxicola infundibulum*. Such an observation at the light microscopy level was also observed by TEM, revealing the presence of an organelle with four membranes close to the anterior part of each *S. hollandei* merozoite (Schrével 1971b).

The apical phagotrophy in the free-living predators of alveolates, with open conoid and rhoptries, may be at the origin of the anchoring device of archigregarines like *Selenidium*, characterized by their mucron and the myzocytosis function. The conoid of *S. pendula*, similar to that of *S. hollandei* (Schrével 1968) and *S. orientale* (Simdyanov and Kuvardina 2007), is conserved in large trophozoites and appears similar to the conoid of sporozoites from eugregarines *Stylocephalus africanus* (Desportes 1969) and *Ascogregarina (Lankesteria) culicis* (Sheffield et al. 1971). Among Conoidasida, the conoid of *T. gondii* is the most investigated at the structural and molecular levels, with the construction of unique coma-shaped tubulin sheets to form a spiral cone-shaped structure (Hu and Murray 2002; Hu et al. 2006). As *S. pendula* is the archigregarine type species and an early branching Apicomplexa, its conoid appears a good model to study the transition between Apicomplexa with closed conoid and free-living alveolate ancestors with open conoid, as found in the early branching dinoflagellates as *Colpodella* (Brugerolle 2002; Leander et al. 2003) or *Psammosa pacifica* (Okamoto and Keeling 2014).

Recently, the hypothesis of molecular links between Apicomplexa and algal ancestors was suggested with the demonstration of similar components in the apical complex of Myzozoa and the flagellar apparatus of protists. This hypothesis was mainly supported by the localization of striated fiber assemblies (Francia et al. 2012) and SAS-6 proteins (de Leon et al. 2013). *T. gondii* striated fiber assemblins (TgSFA2 and TgSFA3) proteins whose orthologs are found in the rootlet associated with the basal bodies from green algae, polymerize into a dynamic fiber that emerges from the centrosomes immediately after their duplication (Francia et al. 2012). Genetic experiments showed that the two proteins TgSFA2 and 3 play an essential role in the cell division of the *T. gondii*

since cytokinesis is blocked in their absence. This Tg SFA fiber thus provides a robust spatial and temporal organizer for the parasite cell division. Also, Francia et al. (2012) indicated that other comparable SFA fibers were observed in previous ultrastructural studies on *Eimeria* (Dubremetz 1973, 1975) and *Plasmodium* (Schrével et al. 2008).

The SAS-6 protein is well known in the centriolar biogenesis of eukaryotes from protists to vertebrates (Leidel et al. 2005; van Breugel et al. 2011). This protein was described in the centrocone during *T. gondii* cryptomitosis (de Leon et al. 2013). In addition a novel SAS-6 like (SAS-6L) protein family that shares an N-terminal domain with SAS-6 but without the coiled-coil tails was localized above the *T. gondii* conoid (de Leon et al. 2013). Genomic analyses showed that SAS-6L is an ancient protein found in diverse eukaryotic lineages: *Trypanosoma, Leishmania*, ciliates and Apicomplexa (Hodges et al. 2010; de Leon et al. 2013). In *Trypanosoma brucei* trypomastigotes, the Tb SAS-6L was observed near the basis of the flagellum, consistent with the basal body location. In *T. gondii,* the Tb SAS-6L antibody labelled the apex of tachyzoites, and after conoid extrusion triggered by ionomycin treatment, it labelled the tip of the "true" conoid. The SAS-6L and SAS-6 antibodies did not colocalize in *T. gondii*, the former one labelling the centriole and the latter one labelling the conoid tip (de Leon et al. 2013).

Complex connections between the "pseudoconoid" or "incomplete conoid" and the flagellar apparatus were also shown, by conventional TEM and 3D reconstruction, in the apical complex of *Psammosa pacifica,* a predator relative of apicomplexans and early dinoflagellates (Okamoto and Keeling 2014).

The MTOC of the centrocones of *S. pendula* appears as a disc similar to that observed in other eugregarines such as *L. tuzetae* where 9 singlets could be detected in favourable TEM sections (Kuriyama et al. 2005). From these MTOC discs, microtubules radiated to form a cone involved in the cup-shaped invaginations of the nuclear envelope. The continuity of these MTOC during the life cycle could be in agreement with a centriolar-like structure since a 9+0 axonemal pattern is observed in *S. pendula* male gamete (Fig.11B). The question of the subpellicular microtubule biogenesis is not clear. The conoid is not, by itself, the MTOC since it is absent in the zoites of Hematosporida and Piroplasmida. The two polar rings, observed at the apex of the *Eimeria* or *Plasmodium* zoites were proposed as the MTOC sites generating the subpellicular microtubules (Russel and Burns 1984), but these two polar rings were not observed in *S. pendula*. The imc dilatation at the border of the proximal opening of the conoid could fulfil this function (Fig. 4). The exceptional accumulation of microtubule bundles in the anterior part of the mucron,

before the regular subpellicular microtubule sets of the epicytic bulges (Fig. 2D), is in agreement with the strong labelling of *S. melongena* apex with fluorescent anti-alpha tubulin (Wakeman et al. 2014). Biogenesis of these abundant microtubule bundles needs further analysis.

Rhoptries are characteristic of the apicomplexan zoites and also of the Selenidiidae trophozoites (Schrével et al. 2013 for a review). Interestingly, presence of numerous intracytoplasmic thread-like bodies described by Ray (1930) in the apex of different *Selenidium* trophozoites was visualized after iron haematoxylin staining (Heidenhain's haematoxylin). By their sizes reaching 8-12 µm depending on the *Selenidium* species and their localization, these thread-like structures could correspond to the rhoptries described from TEM such as in *S. pendula* (Fig. 5A), *S. hollandei* (Schrével 1968) and *S. orientale* (Symdyanov and Kurvidina 2007). Ray (1930) considered these thread-like structures as one of the morphological characters of each *Selenidium* species, however the abundance of rhoptries detected in TEM is in fact a general character for archigregarines (Schrével et al. 2013, for review). Biological functions of many apicomplexan rhoptry proteins remain largely unknown. In *Plasmodium* and *Toxoplasma*, the most investigated apicomplexans at the molecular level, there is growing evidence to suggest that the rhoptry neck proteins are predominantly involved in host-cell adhesion with some sharing evolutionary origins among apicomplexans. In contrast, the rhoptry bulb proteins appear mainly genus specific, suggesting that they evolved secondarily to become highly specific to their host cells (Counihan et al. 2013). In *S. pendula,* food vacuole membranes may have arised from numerous rhoptries localized within the apex. A strong membrane trafficking is expected to produce the large and abundant food vacuoles observed during myzocytosis (Fig. 4A). Therefore *Selenidium* rhoptry proteins could play a role in producing intracellular food vacuole in contrast to Apicomplexa with an intracellular development, where the rhoptry proteins seem involved in the parasitophorous vacuole elaboration such as in *Plasmodium* and *Toxoplasma.*

Archigregarines and Eugregarines: Two Early Branching Lineages Among Apicomplexa

The transition from the free-living alveolates to apicomplexan parasites was supported by comparative ultrastructural studies and molecular phylogeny analyses of basal lineages, such as dinoflagellates (together with perkinsids) and apicomplexans (including colpodellids) (Leander and Keeling 2003). The myzocytosis is the most plesiomorphic

features of apicomplexans with archigregarines having a closed conoid (Schrével 1968, 1971b), and colpodellids the sister lineage of Apicomplexa with an open conoid (Kuvardina et al. 2002). In perkinsids, representing the earliest diverging sister lineage of dinoflagellates (Saldarriaga et al. 2003), an open conoid is also observed (Perkins 1996). These three types of parasites also share rhoptry-like organelles and, together with their phylogenetic positions, they confidently infer that a common ancestor of apicomplexans and dinoflagellates had an apical complex involved in the acquisition of nutrients from the cytoplasm of prey cells (Leander and Keeling 2003).

Among the high diversity of gregarines in invertebrates, Polychaeta, an animal class known to be present at the Cambrian biodiversity explosion and to represent one of the earliest Bilateria organisms (De Rosa et al. 2005; Schrével and Desportes 2013), is well infected by gregarines. This situation supports the evolutionary prelude of marine gregarines to the apicomplexan radiation (Leander 2007). The initial archigregarine radiation is supported by the "hypersporozoite" cell organization of the trophozoite, the myzocytosis and the pendular or rolling motility (Schrével 1971; Schrével and Desportes 2015). The subsequent eugregarine radiation, with an adaptation to the intestinal biome and an extracellular development, could have emerged from intestinal lecudinid gregarines. Here, their cell cortex is quite different from archigregarines by the presence of numerous epicytic folds, without the regular sets of subpellicular microtubules but with a sophisticated distribution of 12-nm filaments, apical rippled dense structures at the top of the folds (Schrével et al. 1983;Vivier 1968). Their gliding motility depends upon an actin-myosin system but the molecular mechanochemical properties are far from being understood (Heintzelman 2004; Valigurová et al. 2013). The myzocytosis, similar to the archigregarine model, is not observed in these marine eugregarines: their nutrition process is realized through a bulbous attachment apparatus usually designated by mucron.

The gregarine colonization of the coelom in invertebrate hosts by transmigration of the sporozoites through the intestinal epithelium and a coelomic development reveal additional adaptations of eugregarines to their host environment. These adaptations are a significant evolutionary step of marine gregarines as suggested by Leander (2007), and represent an antithesis to any notion of "primitiveness". One of the best evidence is the unique adaptation of the coelomic eugregarine *Diplauxis hatti* to its host *Perinereis cultrifera* where a strict synchronization is observed between the maturation of the polychaete gametes and the sexual phases (gamogony and sporogony) of the parasite (Prensier et al. 2008). This example illustrates how gregarines are well adapted to their host

environment. For instance, *D. hatti* is adapted to *P. cultrifera* but cannot invade other Nereidae host as *Hedistes (Nereis) diversicolor* nor *Nereis pelagica*. The extreme adaptation of some gregarines to their host environments could explain some unexpected situations such as the reduction observed from the canonical 9+2 flagellar pattern, in the male gametes, with a 9+0 pattern in *S. pendula* (this study), 6+0 in *L. tuzetae* (Schrével and Besse 1975) and 3+0 in *D. hatti* (Prensier et al. 1980). The 9+0 pattern of *Selenidium*, close to the 9+2 normality, may be correlated to a fertilization phase lasting about 1 hour in a 1-day sexual phase (gamogony and sporogony), the 6+0 pattern of *L. tuzetae,* may result from a fertilization realized in few hours within a cyst, during a 3 days sexual phase of the *Lecudina* life cycle (Schrével 1969). More impressively, the 3+0 pattern in *D. hatti* could have been selected over evolution because of the fertilization step lasting only few hours in a highly extended complete life cycle, lasting 2.5 years (Prensier et al. 2008). Such evolutionary proposal, suggesting that each gregarine develops its own programme according to its environment is in agreement with the notion of regressive evolution in microorganisms proposed by Lwoff (1944). This type of regressive evolution could probably continue with other coelomic gregarines with the disappearance of the flagellum in male gametes of *Gonospora* species as suggested from histology studies (Schrével 1963; Trégouboff 1918). Expression of the own program of each coelomic eugregarines is also observed with the variations in their epicytic cell surface transformations with digits, surface swelling in *Pterospora*, microvillosities in *Diplauxis* or the development of peristaltic motility instead of gliding, sometimes a pendular motility is observed in young trophozoite and peristaltic motility during the fast growing period of the same trophozoite as observed in *D. hatti* (see Schrével et al. 2013 for a review).

Conclusion

Molecular phylogenetic analyses of archigregarines demonstrate that *S. pendula,* the type species of archigregarines, belongs to a lineage with a large number of *Selenidium* parasites of Spionidae, Sabellaridae, Sabellidae, Cirratulidae families of the Sedentaria Polychaeta. All these *Selenidium* exhibit similar biological characters such as the cell cortex with a plasma membrane, imc (inner-membrane-complex) and subpellicular microtubules, the apical complex with a conoid, the myzocytosis with large food vacuoles and abundance of

large rhoptry organelles, the nuclear multiplication during the syzygy and the early gamonts. Two other *Selenidium*-like lineages are observed in the Terebellidae and Sipunculida where the sexual characters are not available at this time. Such a status underlines an adaptation of the family Selenidiidae to their host families and this first early evolutive lineage could correspond to the transition step between the free-living flagellated alveolates and the Apicomplexa, before the diversification of the marine eugregarines without the typical myzocytosis realized through the conoid but with a gliding motility.

Methods

Preparation of annelids and gregarines: Isolates of the gregarine *Selenidium pendula* Giard, 1884 type species, were collected from the intestine of the polychaete worm *Scolelepis squamata* (O. F. Müller, 1806) (previously named *Nerine cirratulus,* Delle Chiaje, 1831) on the French coast of the English Channel at the "Station Biologique de Roscoff", in 2007 then again in 2012. Isolates of the gregarines *Selenidium hollandei* Vivier and Schrével, 1966, *Lecudina pellucida* (Mingazzini, 1891) type species and different isolates of *L. tuzetae* Schrével, 1963 were also collected from the intestines of polychaete worms from the same area, in 2007, 2012, 2013 and 2014 (Table 2).

After washing in seawater, each collected worm was kept, at the laboratory temperature, in a separate Petri dish. The medium (seawater) was changed daily. For long-term conservation, the collected worms were rinsed with 0.22 µm filtered seawater and stored at 4 °C. In order to collect *Selenidium pendula* Giard, 1884, the anterior part of the *Scololelepis squamata* worms, with a yellow color, was discarded since the parasites were always absent, then the worms were cut transversally in series of segments of about 1 to 1.5 cm of length. To collect *S. hollandei*, *L. pellucida* and *L. tuzetae*, a similar type of microdissection was performed from their corresponding hosts, under a classic binocular microscope, in order to expose the intestinal epithelial surface to the seawater. In addition, and only in the case of *L. tuzetae,* cysts excreted with feces were collected from the Petri dishes of individually kept *Neanthes (Nereis) diversicolor* (O. F. Müller, 1776). Trophozoites of *S. pendula*, attached to the intestine, were easily detected, in spite of their rather small sizes (usually 150 -180 µm x 30-35 µm), by their white color - contrasting to the characteristic green color of the intestinal epithelium of the worm - and by their active

pendular movements. In highly infected *Scolelepis squamata*, trophozoites and sexual stages of *S. pendula* (syzygies and young cysts) were also collected in Petri dishes, among the gametes released from hosts during the dissection. *S. hollandei* trophozoites were easily observed in host epithelium by their very active rolling movements, immediately after sectioning the post abdominal segment of their hosts, *Sabellaria alveolata* Linnaeus, 1767.

Electron microscopy: For transmission electron microscopy (TEM), intestinal epithelial tissues of *Scolelepis squamata* highly infected with trophozoites of *S. pendula* were collected and fixed in 5 % (v/v) glutaraldehyde in 100-150 mM phosphate or 0.2 M cacodylate buffer (pH 7.3), at 4 °C, for 6 to 12 hours. The syzygy and gametocytes of *S. pendula,* not attached to the epithelium, were collected directly in the seawater from the Petri dishes and fixed in the same conditions. After washing either in the same buffer or in buffer containing 0.3 M sucrose, the samples were post-fixed with 1% (w/v) OsO_4 in the same buffer for 1 hr, then processed through standard dehydration, infiltration, and embedding procedures, in Epon or Araldite mixtures, with the corresponding solvents (i.e. propylene oxide or acetone respectively), at room temperature. The blocks were thin sectioned, collected on grids and stained with saturated uranyl acetate in 50% (v/v) ethanol for 1-3 min then in lead citrate. Sections were observed with a Hitachi HU 11 E electron microscopy (Hitachi Ltd, Japan) or a JEOL 1010 TEM.

For SEM, the intestines were open along the axis of the polychaete, and the body parts highly infected by *S. pendula* were carefully washed in 0.22 µm-filtered seawater before fixation in glutaraldehyde as done above for TEM. After the post fixation in 1% OsO_4 in 0.2 M cacodylate buffer, specimens were dehydrated in a graded series of acetone, critical point-dried in liquid CO_2 and coated with gold. The samples were examined in a JEOL JSM-7401F FE SEM.

DNA isolation and sequencing: For the LG isolates (*S. pendula* LG, *S. hollandei* LG, *L. pellucida* LG Table 1), groups of ~50-70 isolated trophozoites were washed at least three times in 0.22 µm-filtered seawater and DNA was extracted from individual parasites using a modified GITC (Guanidinium isothiocyanate) protocol (Chomczynski and Sacchi 2006). Individuals were placed in 50 µl of the GITC extraction buffer and crushed using an adjusted micro-pilon (Kimble Chase®). Tubes were incubated at 72 °C for 20 min. Next, one volume of cold isopropanol was added at −20 °C overnight for DNA precipitation. The following day, samples were centrifuged (20,000 ***g*****,** 15 min at 4 °C) and supernatants removed. The DNA pellet was cleaned using 70% ethanol (100 µl), followed by a last centrifugation (20,000 *g*, 10 min). Supernatant was removed and the DNA pellet was

hydrated into 20 µl of sterile distilled water and stored at −20 °C. For *S. pendula* IF, a group of ~50-70 isolated trophozoites were washed at least three times in 0.22 µm filtered seawater and genomic DNA was isolated by using a phenol-chloroform extraction procedure as previously described for *Plasmodium falciparum* (Florent et al. 2000), and the purified DNA pellet was rehydrated into 20 µl of sterile distilled water and stored at -20 °C.

For *L. tuzetae* Roscoff 2012 IF462, DNA was isolated by using the phenol-chloroform extraction procedure described above, from 2 cysts, collected from the feces of a single *Neanthes (Nereis) diversicolor* (O. F. Müller, 1776) host individually kept in a Petri dish. The purified DNA pellet was rehydrated into 20 µl of sterile distilled water and was stored at -20 °C. Finally, for the 4 remaining *L. tuzetae* Roscoff, DNA extractions were performed using MasterPure^{TM} Complete DNA and RNA Purification kit (Epicentre, Illumina Inc. USA) following supplier's recommendations for Cell Samples manipulations, with minor modifications, from respectively 7 cysts (IF131), 50 cysts (IF171 and IF172) and 30 cysts (IF181). Briefly, each group of cysts was isolated from the feces of a single *N. diversicolor* host individually kept in a Petri dish, from which each cyst was then extensively washed, one by one, in three successive drops of 0.22 µm filtered seawater supplemented with antibiotics penicillin (100 U/mL), streptomycin (100 µg/mL) and gentamycin (50 µg/mL) (Gibco, Life Technologies, USA) then pooled again. Then, isolated and washed cysts were submerged in 300 µL Tissue-and-Cell lysis solution, submitted to five series of freezing (liquid nitrogen) and thawing (37 °C) before addition of Proteinase K then RNAse A and, after sample processing as recommended, isolated DNA pellets were rehydrated in 35 µl TE (10 mM Tris-pH 7.5 and 1mM EDTA) prior to subsequent storage at -20 °C.

These DNA extraction products were then used as templates in various series of PCR amplifications, in order to amplify the SSU rRNA gene of these gregarines, then sequenced using the Sanger sequencing methodology.

LG samples. The PCR mix (15 µl final volume) contained 1–6 µl of the DNA extract, 330µM of each deoxynucleoside triphosphate (dNTP), 2.5 mM of $MgCl_2$, 1.25 U of GoTaq® DNA polymerase (Promega Corporation), 0.17 µM of both primers, 1× of buffer (Promega Corporation). The PCR cycle, run in an automated thermocycler (GeneAmp®PCR System 9700, Applied Biosystem, USA), was programmed to give an initial denaturating step at 95 °C for 5 min, 35 cycles of denaturating at 95 °C for 1min, annealing at 55 °C for 45 s and extension at 72 °C for 1 min 15 s, and a final extension step at 72 °C for 7 min. PCR products were cloned into a TOPO TA cloning kit (Invitrogen®),

following manufacturer's recommendations. Inserts inside white colonies were screened by PCR (same procedure as before). Positive PCR products were purified (ExoSAP-IT® For PCR Product Clean-Up, USB®) and sequenced using the Big Dye Terminator Cycle Sequencing Kit version 3.0 (PE Biosystems®) and an ABI PRISM model 377 (version 3.3) automated sequencer with specific internal primers.

The list of primers used for both PCR amplifications and Sanger sequencing is provided in the table of the Supplementary data 6.

IF samples. PCR amplifications were done using Hot firepol DNA polymerase as recommended (Solis BioDyne, Estonia), in a 50 µl final volume supplemented with 2 mM $MgCl_2$, 200 µM each dNTPs and 200 nM forward (P4+T or WL1) and reverse (EukP3) primers (Supplementary Material 6) and 1µl of isolated gregarine DNAs. PCR cycles, run in an automated thermocycler (GeneAmp®PCR System 9700, Applied Biosystem, USA), were programmed to give an initial denaturation step at 95 °C for 4 min, 30 cycles of denaturation at 95 °C for 30 s, annealing at 51°Cfor 30 s and extension at 72 °C for 2 min, and a final extension step at 72 °C for 7 min. PCR products were purified using Illustra™ GFX™ PCR DNA and Gel Band Purification kit (GE Healthcare, France) and were cloned into pGEM®-T Easy vector (Promega, Madison WI, USA) using supplier's recommendations. DNA sequences were obtained from positive clones selected by PCR using T7 and Sp6 universal primers flanking the pGEM®-T Easy vector cloning site, using T7, Sp6 and internal primers such as LWA1, LWA3, PIF3F and PIF3R (Table 6), by the Sanger method (Beckman Coulter Genomics, Takeley, UK). Raw were edited using the BioEdit 7.1.3.0 program (Hall 1999) and assembled by using MEGA6 (Tamura et al. 2013).

Phylogenetic analyses: SSU rDNA sequences from nine *Selenium* and *Lecudina* species were aligned to 106 rDNA sequences from diverse eukaryotes, mostly corresponding to representatives of Alveolata with one Rhizaria as outgroup. Sequences were aligned using the online version of MAFFT version 7 (http://mafft.cbrc.jp/alignment/server/ Katosh and Toh 2010), using the secondary structure of RNA (Q-INS-I option) and further refined manually taking as a reference the secondary structure of *T. gondii* small subunit rRNA (Gagnon et al. 1996). Ambiguously aligned positions were manually removed which yielded a confident alignment of 1350 positions. A GTR substitution model with gamma-distributed rate variation across sites was suggested as the best-fit model by JModeltest V2.1.3 (Darriba et al. 2012). Accordingly, a Bayesian phylogenetic tree was constructed with MrBayes v.3.2.3 (Ronquist et al. 2012) using lset nst=6 rates=Invgamma Ngammacat=4 parameters. Four simultaneous Monte

Carlo Markov chains were run from random trees for a total of 13,000,000 generations in two parallel runs. A tree was sampled every 1000 generation and 25% of the trees were discarded as "burn-in". A consensus tree was constructed from the post-burn-in trees and posterior probabilities were calculated in MrBayes. Maximum Likelihood analyses were performed with MEGA 6.06 (Tamura et al. 2013) using the GTR+G+I model. Bootstraps were estimated from 1,000 replicates.

The phylogenetic tree for the Selenidiidae lineage from polychate annelids (Fig. 13) was contructed using the same alignment but for a subset of 20 sequences; all position containing gaps and missing data were eliminated; there were a total of 1,416 positions in the final dataset. Maximum Likelihood analyses were performed with MEGA 6.06 (Tamura et al. 2013) using the GTR+G+I model. Bootstraps were estimated from 1,000 replicates.

Estimate of evolutionary divergence between sequences: Evolutionary divergence between sequences was computed by using the MEGA 6.06 (Tamura et al. 2013) using a subset of sequences extracted from the main phylogenetic alignment. For the analysis of the Selenidiidae lineage (Supplementary Material 4) the analysis involved 33 nucleotide sequences for 16 distinct species, there were a total of 2088 positions in the final dataset and all positions containing gaps and missing data were eliminated.

Acknowledgements

Many thanks to Dr Isabelle Desportes (MNHN) for her fruitful comments, Dr Marc Dellinger (MNHN) for help in primer design and Dr Marc Gèze (MNHN) for imaging on the MNHN-CEMIM Platform. The careful illustrations of the figures were realized by Doanh Baccam (MNHN). This study was supported by ECO-NET Project 2131QM (Égide, France), PHC-Barrende projects 24663ND (2011-2012) and 31266SL (2014-2015), Interdisciplinary Programs of the MNHN (ATM-Microorganismes, ATM-Emergence des clades, des biotes et des cultures) and by the French governmental ANR under ANR-10-LABX-0003 BCDiv, ANR-11-IDEX-0004-0 and the ANR-14-CE02-0007-01 (HAPAR). AV was funded by the Czech Science Foundation project No. GBP505/12/G112 (ECIP), and her travel expenses were supported by projects MEB021127 and 7AMB14FR013 from the Ministry of Education, Youth and Sports of the Czech Republic.

References

Boothroyd JC, Dubremetz JF (2008) Kiss and split: the dual roles of *Toxoplasma* rhoptries. Nat Rev Microbiol **6**:79-88

Bradley PJ, Ward C, Cheng SJ, Alexander DL, Coller S, Coombs GH, Dunn JD, Ferguson DJ, Sanderson SJ, Wastling JM, Boothroyd JC (2005) Proteomic analysis of rhoptry organelles reveals many novel constituents for host-parasite interactions in *Toxoplasma gondii*. J Biol Chem **280**:34245-34258

Brasil L (1907) Recherches sur le cycle évolutif des *Selenidiidae*, Grégarines parasites d'Annélides polychètes. I. La schizogonie et la croissance des gamétocytes chez *Selenidium caulleryi* n. sp. Arch Protistenkd **16**:370-397

Brugerolle G (2002) *Colpodella vorax*: ultrastructure, predation, life-cycle, mitosis, and phylogenetic relationships. Eur J Protistol **38**:113-125

Caullery M, Mesnil F (1899) Sur quelques parasites internes des Annélides. I. Grégarines nématoides des annélides. Trav Stat Zool Wimereux **7**:80-99

Caullery M, Mesnil F (1900) Sur un mode particulier de division nucléaire chez les Grégarines. Arch Anat Microsc **3**:146-167

Chomczynski P. and Sacchi, N (2006) The single-step method of RNA isolation by acid guanidinium thiocyanate-phenol-chloroform extraction: twenty-something years on. Nat Protoc **1**:581–585

Counihan NA, Kalanon M, Coppel RL, de Koning-Ward TF (2013) *Plasmodium* rhoptry proteins: why order is important. Trends Parasitol **29**:228-236

Darriba D, Taboada GL, Doallo R, Posada D (2012) jModeltest 2: more models, new heuristics and parallel computing. Nat Methods **9**:772-772

de Leon JC, Scheumann N, Beatty W, Beck JR, Tran JQ, Yau C, Bradley PJ, Gull K, Wickstead B, Morisette NS (2013) A SAS-6-like protein suggests that the *Trypanosoma* conoid complex evolved from flagellar components. Eukaryot Cell **12**:1009-1015

De Rosa R, Prud'homme B, Balavoine G (2005) Caudal and even-skipped in the annelid *Platynereis dumerilii* and the ancestry of the posterior growth. Evol Dev **7**:574-587

Desportes I, Schrével J (2013, eds) The Gregarines: The Early Branching Apicomplexa. Brill, Leiden, 781 p

Dubremetz JF (1973) Etude ultrastructurale de la mitose schizogonique chez la Coccidie *Eimeria necatrix* (Johnson, 1930). J Ultrastruct Res **42**:354-376

Dubremetz JF (1975) Genesis of merozoites in the coccidia, *Eimeria necatrix*: Ultrastructural study. J Protozool **22**:71-84

873 **Florent I, Mouray E, Dali Ali F, Drobecq H, Girault S, Schrével J, Sergheraert C,**
874 **Grellier P** (2000) Cloning of *Plasmodium falciparum* protein disulfide isomerase
875 homologue by affinity purification using the antiplasmodial inhibitor inhibitor 1,4-bis{3-
876 [N-(cyclohexyl methyl)amino]propyl}piperazine. FEBS Lett **484**:246-252
877 **Francia ME, Jordan CN, Patel JD, Sheiner L, Demerly JL, Fellows JD, de Leon JC,**
878 **Morrissette NS, Dubremetz JF, Striepen B** (2012) Cell division in apicomplexan
879 parasites is organized by a homolog of the striated rootlet fiber of algal flagella. PLoS Biol
880 10:e1001444
881 **Francia ME, Striepen B** (2014) Cell division in apicomplexan parasites. Nat Rev
882 Microbiol **12**:125-136
883 **Gagnon S, Bourbeau D, Levesque RC (1996)** Secondary structures and features of the
884 18S, 5.8S and 26S ribosomal RNAs from the apicomplexan parasite *Toxoplasma gondii*.
885 Gene **173**:129-35
886 **Goldstein SF, Schrével J** (1982) Microtubules and cell motility. SFRS, France,
887 CERIMES, www.cerimes.education.fr
888 **Gunderson J, Small EB** (1986) *Selenidium fallax* n.sp. (Protozoa, Apicomplexa) from the
889 sipunculid *Phascolosoma agassizii* Kerferstein 1867. J Parasitol **72**:107-110
890 **Hall TA** (1999) BioEdit: a user-friendly biological sequence alignment editor and analysis
891 program for Windows 96/98NT. Nucleic Acids Symp Ser **41**:95-98
892 **Harper JD, Thuet J, Lechtreck KF, Hardham AR (2009**) Proteins related to green algal
893 striated fiber assemblin are present in stramenopiles and alveolates. Protoplasma **236**:97-
894 101
895 **Heintzelman MB** (2004) Actin and myosin in *Gregarina polymorpha.* Cell Motil
896 Cytoskeleton **58**:83-95
897 **Hodges ME, Scheumann N, Wickstead B, Langdale JA, Gull K** (2010) Reconstructing
898 the evolutionary history of the centriole from protein components. J Cell Biol **123**:1407-
899 1413
900 **Hoshide H, Todd KS (1996)** The fine structure of cell surface and hair-like projections of
901 *Filipodium ozakii* Hukui. Acta Protozool **35**:309-315
902 **Hu K, Roos DS, Murray JM** (2002) A novel polymer of tubulin forms the conoid of
903 *Toxoplasma gondii*. J Cell Biol **156**:1039-1050
904 **Hu K, Johnson J, Fraunholz M, Surajajjala S, DiLullo C, Yates J, Rossn DS, Murray**
905 **JM** (2006) Cytoskeletal Components of an Invasion Machine-The Apical Complex of
906 *Toxoplasma gondii.* PLoS Pathogens **2**(2):e13:121-138

907 **Katoh K, Toh H** (2010) Parallelization of the MAFFT multiple sequence alignment
908 program. Bioinformatics **26**:1899-1900
909 **Kuriyama R, Besse C, Geze M, Omoto CK, Schrével J** (2005) Dynamic organization of
910 microtubules and microtubule-organizing centers during the sexual phase of a parasitic
911 protozoan, *Lecudina tuzetae* (Gregarine, Apicomplexa). Cell Motil Cytoskeleton **62**:195-
912 209
913 **Kuvardina ON, Leander BS, Aleshin VV, Myl'nikov AP, Keeling PJ, Simdyanov TG**
914 (2002) The phylogeny of colpodellids (Alveolata) using small subunit rRNA genes
915 sequences suggests there are the free-living group to apicomplexans. J Eukaryot Microbiol
916 **49**:498-504
917 **Leander BS (**2006) Ultrastructure of the archigregarine *Selenidium vivax* (Apicomplexa)-A
918 dynamic parasite of sipunculid worms (host: *Phascolosoma agassizii*). Mar Biol Res **2**:178-
919 190
920 **Leander BS** (2007a) Marine gregarines: evolutionary prelude to the apicomplexan
921 radiation? Trends Parasitol **24**:60-7
922 **Leander BS** (2007b) Molecular phylogeny and ultrastructure of *Selenidium serpulae*
923 (Apicomplexa, Archigregarinia) from the calcareous tubeworm *Serpula vermicularis*
924 (Annelida, Polychaeta, Sabellida). Zool Scripta **36**:213-22
925 **Leander BS, Keeling PJ** (2003) Morphostasis in alveolate evolution. Trends Ecol Evol
926 **18**:395-404
927 **Leander BS, Harper JT, Keeling PJ** (2003) Molecular phylogeny and surface
928 morphology of marine aseptate gregarines (Apicomplexa): *Selenidium* spp. and *Lecudina*
929 spp. J Parasitol **89**:1191-205
930 **Leander BS, Kuvardina ON, Aleshin VV, Mylnikov AP, Keeling PJ** (2003) Molecular
931 phylogeny and surface morphology of *Colpodella edax* (Alveolata): insights into the
932 phagotrophic ancestry of apicomplexans. J Eukaryot Microbiol **50**:334-340
933 **Léger L, Duboscq O** (1917) Sporozoaires de *Glossobalanus minutus* Kow. *Eimeria*
934 *epidermica* n. sp.; *Eimeria beauchampi* n. sp.; *Selenidium metchnikowi* n. sp. Ann Inst
935 Pasteur **31**:60-74
936 **Leidel S, Delattre M, Cerutti L, Baumer K, Gonczi P** (2005) SAS-6 defines a protein
937 family required for centrosome duplication in *C. elegans* and human cells. Nat Cell Biol
938 **7**:115-125
939 **Lim L, McFadden GI** (2010) The evolution, metabolism anf functions of the apicoplast.
940 Philos Trans Royal Soc B 365:749-763

Lwoff A (1944) L'évolution physiologique. Etude des pertes de fonction chez les microorganismes. Hermann Publ, Paris, 308 p

Macgregor HC, Thomasson PA (1965) The fine structure of two archigregarines, *Selenidium fallax* and *Ditrypanocystis cirratuli*. J Protozool **12**:438-443

Mignot JP (1966) Ultrastructure des Eugléniens. Etude de la cuticule chez différentes espèces. Protistologica **2**:51-117

Misof B, Liu S, Meusemann K, et al. (2014) Phylogenomics resolves the timing and pattern of insect evolution. Science **346**:763-767

Molon-Noblot S, Desportes I (1980) Etude ultrastructurale des mitoses gamogoniques de la Grégarine *Grebnickiella gracilis* Gr. parasite de la scolopendre *Scolopendra cingulata* L. Considérations sur les mitoses schizogoniques des Sporozoaires (Apicomplexa). Protistologica **16**:395-411

Nei M, Kumar S (2000) Molecular Evolution and Phylogenetics. Oxford University Press, New York, 333 p

Okamoto N, Keeling PJ (2014) The 3D structure of the apical complex and association with the flagellar apparatus revealed by serial TEM tomography in *Psammosa pacifica,* a distant relative of the Apicomplexa. PLoS ONE **9**(1):e84653

Perkins FO (1996) The structure of *Perkinsus marinus* (Mackin, Owen and Collier, 1950) Levine, 1978 with comments on the taxonomy and phylogeny of *Perkinsus* spp. J Shellfish Res **15**:67-87

Prensier G, Vivier E, Goldstein S, Schrével J (1980) Motile flagellum with a "3 + 0" ultrastructure. Science **207**:1493-4

Prensier G, Dubremetz JF, Schrével J (2008) The unique adaptation of the life cycle of the coelomic gregarine *Diplauxis hatti* to its host *Perinereis cultrifera* (Annelida, Polychaeta): an experimental and ultrastructural study. J Eukaryot Microbiol **55**:541-53

Ray HN (1930) Studies on some sporozoa in polychaete worms.I. Gregarines of the genus *Selenidium*. Parasitology **22**:370-398

Reed N (1933) Sporogony in *Selenidium mesnili* Brasil, a sporozoan parasite of *Myxicola infundibulum* Mont. Parasitology **25**:402-409

Ronquist F, Teslenko M, van der Mark P, Ayres DL, Darling A, Höhna S, Larget B, Liu L, Suchard MA, Huelsenbeck JP (2012) MrBayes 3.2: efficient Bayesian phylogenetic inference and model choice across a large model space. Syst Biol **61**:539-42

Rouse GW, Fauchald K (1997) Cladistics and Polychaetes. Zool Scripta **26**:139-204

Rueckert S, Leander BS (2009) Molecular phylogeny and surface morphology of marine archigregarines (Apicomplexa), *Selenidium* spp., *Filipodium phascolosomae* n. sp., and *Platyproteum* n. g. and comb. from North-Eastern pacific peanut worms (Sipuncula). J Eukaryot Microbiol **56**:428-439

Russell DG, Burns RG (1984) The polar ring of coccidian sporozoite: a unique microtubule-organizing centre. J Cell Sci **65**:197-207

Saldarriaga JF, McEwan ML, Fast NM, Taylor FJ, Keeling PJ (2003) Multiple protein phylogenies show that *Oxyrrhis marina* and *Perkinsus marinus* are early branches of dinoflagellate lineage. Int J Syst Evol Microbiol **53**:355-365

Santos JM, Lebrun M, Daher W, Soldati D, Dubremetz JF (2009) Apicomplexa cytoskeleton and motors: key regulators in morphogenesis, cell division, transport and motility. Int J Parasitol **39**:153-162

Schrével J (1963) Contribution à l'étude de trois Grégarines parasites d'Annélides Polychètes: *Lecudina elongata* Mingazzini1891; *Lecudina tuzetae* Schrével 1963; *Gonospora varia* Léger 1892. Arch Zool Exp Gén **104**:125-142

Schrével J (1966) Cycle de *Selenidium pendula* Giard 1884, Grégarine parasite de *Nerine cirratulus* Delle Chiaje (Annélide Polychète). Protistologica **2**:31-34

Schrével J (1968) L'ultrastructure de la région antérieure de la grégarine *Selenidium* et son intérêt pour l'étude de la nutrition chez les Sporozoaires. J Microsc Paris **7**:391-410

Schrével J (1969) Recherches sur le cycle des Lecudinidae grégarines parasites d'Annélides Polychètes. Protistologica **5**:561-588

Schrével J (1970) Contribution à l'étude à l'étude des Selenidiidae parasites d'Annélides Polychètes: I. Cycles biologiques. Protistologica **6**:389-426

Schrével J (1971a) Contribution à l'étude à l'étude des Selenidiidae parasites d'Annélides Polychètes:II. Ultrastructure de quelques trophozoites. Protistologica **7**:101-130

Schrével J (1971b) Observations biologiques et ultrastructurales sur les Selenidiidae et leurs conséquences sur la systématique des Grégarinomorphes. J Protozool **18**:448-470

Schrével J, Besse C (1975) Un type flagellaire fonctionel de base 6+0. J Cell Biol **66**:492-507

Schrével J, Desportes I (2013) Introduction: Gregarines among Apicomlexa. Chapter 1, 7-24 in Desportes I, Schrével J (eds) The Gregarines. The Early Branching Apicomplexa. Brill, Leiden, pp 7-24

Schrével J, Desportes I (2015) Gregarines. In Mehlhorn H (ed). Encyclopedia of Parasitology , 4 th edn, Springer, Berlin, Heidelberg, pp 1-47

Schrével J, Caigneaux E, Gros D, Philippe M (1983) The three cortical membranes of the gregarines. I. Ultrastructural organization of *Gregarina blaberae*. J Cell Sci **61**:151-74

Schrével J, Desportes I, Goldstein S, Kuriyama R, Prensier G, Vávra J (2013) Biology of Gregarines and their Host-parasite Interactions. Chapter 2, 25-195 in Desportes I, Schrével J (eds) The Gregarines. The Early Branching Apicomplexa. Brill, Leiden, pp 25-195

Schrével J, Asfaux-Foucher G, Hopkins JM, Vincent R, Bourgouin C, Prensier G, Bannister LH (2008) Vesicle trafficking during sporozoite development in *Plasmodium berghei:* ultrastructural evidence for a novel trafficking mechanism. Parasitology **135**:1-12

Sheffield HG, Garnham PCC, Shiroishi T (1971) The fine structure of the sporozoite of *Lankesteria culicis*. J. Protozool **18**:98-105

Simdyanov TG, Kuvardina ON (2007) Fine structure and putative feeding mechanism of the archigregarine *Selenidium orientale* (Apicomplexa:Gregarinomorpha). Eur J Protistol **43**:17-25

Struck TH, Paul C, Hill N, Hartman S, Hösel C, Kube M, Lieb B, Meyer A, Tiedemann R, Purschke G, Bleidorn C (2011) Phylogenomic analyses unravel annelid evolution. Nature **471**:95-98

Tamura K, Stecher G, Peterson D, Filipski A, Kumar S (2013) MEGA6: Molecular Evolutionary Genetics Analysis Version 6.0. Mol Biol Evol **30**:2725-2729

Toso MA, Omoto CK (2007) *Gregarina niphandrodes* may lack both a plastid genome and organelle. J Eukaryot Microbiol **54**:66-72

Trégouboff G (1918) Etude monographique de *Gonospora testiculi* Treg., grégarine parasite du testicule de *Cerithium vulgatum* Brug. Arch Zool Exp Gén **57**:471-509

Tuzet O, Ormières R (1958) *Selenidium flabelligerae* n. sp. parasite de *Flabelligera diplochaitos* Otto (Annélide sédentaire). Ann Sci Nat Zool **13**:71-76

Valigurová A, Vaškovicová N, Musilová N, Schrével J (2013) The enigma of eugregarine epicytic folds: where the gliding motility originates? Frontiers Zool **10**:57

van Breugel M, Hirono M, Andreeva A, Yanagisawa HA, Yamaguchi S, Nakazawa Y, Morgner N, Petrovitch M, Ebong IO, Robinson CV, Johnson M, Veprintsev D, Zuber B (2011) Structures of SAS-6 suggest its organization in centrioles Science 331:1196-1199

Vivier E (1967) Observations ultrastructurales sur l'enveloppe nucléaire et ses "pores" chez les Sporozoaires. J Microsc Paris **6**:371-390

Vivier E (1968) L'organisation ultrastructurale corticale de la grégarine *Lecudina pellucida*; ses rapports avec l'alimentation et la locomotion. J Protozool. **15**:230-246

Vivier E, Schrével J (1964) Etude au microscope électronique d'une Grégarine du genre *Selenidium* parasite de *Sabellaria alveolata* L. J Microsc Paris **3**:651-670

Vivier E, Schrével J (1966) Les ultrastructures cytoplasmiques de *Selenidium hollandei*, n. sp., Grégarine parasite de *Sabellaria alveolata* L. J Microsc Paris **5**:213-228

Wakeman KC, Leander BS (2012) Molecular phylogeny of Pacific Archigregarines (Apicomplexa), including descriptions of *Veloxidium leptosynaptae* n. gen., n. sp., from the sea cucumber *Leptosynapta clarki* (Echinodermata), and two new species of *Selenidium.* J Eukaryot Microbiol **59**:1-14

Wakeman KC, Leander BS (2013) Molecular phylogeny of marine gregarine parasites (Apicomplexa) from tube-forming polychaetes (Sabellariidae, Cirratulidae and Serpulidae) including descriptions of two new species of *Selenidium*. J Eukaryot Microbiol **60**:514-525

Wakeman KC, Heintzelman MB, Leander BS (2014) Comparative ultrastructure and molecular phylogeny of *Selenidium melongena* n. sp. and *S. terebellae* Ray 1930 demonstrate niche partitioning in marine gregarine parasites (Apicomplexa). Protist **165**:493-511

Figure legends

Figure 1. Scanning and transmission electron microscopy of *Selenidium pendula* trophozoites fixed to the intestine of the polychaete worm *Scolelepis squamata* (**A-B.)**. Abbreviations: bulge (B), dense granule (DG), food vacuole (FV), groove (G), intestinal epithelium (IE), mucron (MU), rhoptry (R). **A.** SEM micrograph of trophozoites with their apical region inserted into the intestinal epithelium, exhibiting on this face about 18 longitudinal bulges separated by grooves. The long filamentous structures covering the intestinal epithelium correspond to ciliary structures (arrows). **B.** Longitudinal TEM section of a trophozoite with the apical end designated as mucron containing a food vacuole and numerous rhoptries. In the intestinal epithelium, the trophozoite preferentially anchors to the host cells enriched in dense granules having mucous secretions.

Figure 2. Apex of the *Selenidium pendula* trophozoite (**A-D**). Abbreviations: bulge (B), conoid (Co), food vacuole (FV), groove (G), intestinal epithelium (IE), microneme (mn), microtubules (mt), microvilli (mv), mucron (MU), rhoptry (R). **A.** SEM micrograph of the apex surface showing that bulges and grooves of the epicyte start from a regular mammiliform area corresponding to the external surface of the mucron. Small folds (arrows) are observed on the bulges located on the internal curvature of the cell **B.** SEM micrograph of intestinal epithelium after the detachment of a mucron, with small microvilli on the periphery, a small hole in the subcentral position (white arrow) and the long ciliary structures (black arrow). **C.** TEM micrograph of a median longitudinal section of the apex with several food vacuoles that enter via the conoid and are surrounded by an accumulation of rhoptries and micronemes. **D.** TEM longitudinal section of the apical region (= trophozoite apex with numerous micronemes and rhoptries) revealing that the subpellicular microtubule bundles start before the differentiation of the epicytic bulges of the cell surface.

Figure 3. Cell surface and cortex of *Selenidium pendula* trophozoite **(A-F).** Abbreviations: bulge (B), groove (G), inner membrane complex (imc), microneme (mn), microtubules (mt), mitochondrion (M), myelin-like structure (st myel), plasma membrane (pm), pore (p), rhoptry (R), vesicle (ves). **A.** SEM view of the cell surface with the apertures of pores along the grooves (arrows). **B-F.** TEM cross sections of the cortex with the plasma membrane, the dilated inner membrane complex and the subpellicular microtubules under the epicytic

bulges (C). In cross section, each microtubule is surrounded by a white hexagonal area. Ectoplasmic organelles in the grooves, connected to the cortical membranes via the imc, contain lamellar structures (arrow in B) or dense material (white arrow in D). These organelles form an annular ring in cross section parallel to the cell surface (white arrow in E) corresponding to the cross section of a micropore or myelin-like structures (F).

Figure 4. Conoid in the *Selenidium pendula* mucron **(A-C).** Abbreviations: dense granule (DG), conoid (Co), food vacuole (FV), food vacuole membrane (fvm), inner membrane complex (imc), host intestinal epithelium (IE), parasite plasma membrane (pm). **A-B.** Two longitudinal sections of the *S. pendula* mucron, showing the conoid structure and the opening, allowing a contact between the fvm and the host cell, visible in **A. C.** High magnification showing the 9 cross sections of the microtubular network forming the conoid.

Figure 5. Food vacuoles and rhoptries in the apex of the *S. pendula* trophozoite (**A-B**), and apicoplast-like organelles (**C, D, E**). Abbreviations: conoid (Co), food vacuole (FV), host intestinal epithelium (IE), microneme (mn), mitochondrion (M), fragmented food vacuoles similar to pinocytotic vesicles (pv), rhoptry (R). **A.** TEM cross section with the initial food vacuole passing through the conoid and the fragmented food vacuoles similar to the pinocytotic vesicles (pv) observed in *S. hollandei* (Schrével 1968). Numerous rhoptries are accumulated around these food vacuoles. **B.** Another cross section showing the irregular shapes of the initial food vacuole and the intravacuolar vesicles. **(C-E).** Apicoplast-like organelles, characterized by the presence of four membranes morphologically similar to the apicoplast of *Toxoplasma* and *Plasmodium.*

Figure 6. Rhoptries, micronemes and Golgi apparatus **(A-D).** Abbreviations: amylopectin granule (am), Golgi apparatus (Go), intrareticular granule (ig), microneme (mn), mitochondrion (M), rhoptry (R). **A-B.** TEM cross sections of an accumulation of rhoptries and micronemes within the cytoplasm. The micronemes appear as long-necked bottles, the necks appear as dense rings in cross sections (white thick arrow in B). **C-D.** Golgi apparatus and mitochondrion occur close to the micronemes; the *cis*-region of the Golgi apparatus usually contains numerous intrareticular granules (D).

Figure 7. Nuclear area of *Selenidium pendula* trophozoite **(A-E).** Abbreviations: amylopectin granule (am), intrareticular granule (ig), microneme (mn), nuclear pores (np), nucleus (N), nucleolus (nu). **A-B.** TEM cross sections of the nucleus containing a spherical nucleolus (A) and surrounded by the regular fibrillar zone without organelles (white arrows in B). This fibrillar area is delimited by large vesicles of the rough endoplasmic reticular containing numerous granules and amylopectin granules. **C.** Tangential section of the nuclear envelope exhibits numerous pores. **D.** Occasional accumulation of micronemes can be observed near the nucleus. **E.** Higher magnification of the micronemes and intrareticular granules.

Figure 8. Nuclear development during the syzygy of *Selenidium pendula* **(A-D).** Abbreviations: nucleus (N), cyst wall (CW). **A-B.** Fluorescence staining with DAPI showing nuclei in the median plane of each gamont corresponding to the initial position of the nucleus at the beginning of the syzygy stage. Their numbers are quite similar in the two gamonts and some bright spots are observed in some nuclei (B). **C-D.** TEM cross sections in an early cyst where the nuclei are accumulating in the central position of the gamont while the cell wall is not secreted (C) and later after the secretion of the cyst wall where the nuclei migrate to the gamont periphery (D).

Figure 9. Centrocones and mitosis stages during the gametogenesis of *Selenidium pendula* **(A-B).** Abbreviations: centrocone (CC), chromatin (Ch), cyst wall (CW), dense layer (dl), filamentous layer (fl), nuclear envelope (en), mitochondrion (M), microtubule-organizing center (MTOC), microtubule (mt), nucleus (N), vesicle type 1 (V1) and type 2 (V2). **A.** Early gametogenesis stage before the secretion of the gametocyst wall exhibiting centrocone where the microtubules radiate from the MTOC to the cupule of the nuclear envelope forming a truncated cone. The chromatin covers the inner face of the nuclear envelope and a dense accumulation is observed in the nucleus. **B.** A second centrocone migrating on the other side of the nucleus. No intranuclear spindle is observed, the chromatin is attached to the persistent nuclear envelope. Two types of vesicles are observed one with dense granules (V1) and a second one with filamentous material (V2). The gametocyst wall exhibits an external filamentous layer and an internal dense layer.

Figure 10. Reorganisation of the cortical membranes in *Selenidium pendula* gamonts and ultrastructure of the gametocyst wall during the gametogenesis stage **(A-D).** Abbreviations:

gametocyst wall (CW), dense layer (dl), epicytic folds (ef), filamentous layer (fl), inner membrane complex (imc), plasma membrane (pm), vesicle type 1 (V1) and type 2 (V2). **A-C.** TEM cross sections of the gamont's periphery where the epicytic folds are disorganized with dissociation of the inner member complex under the plasma membrane. The wall of the gametocyst exhibits a filamentous external layer and a more homogenous internal layer; the vesicles of type 2 are probably involved in the cyst wall construction. **D.** Higher magnification of the cyst wall with large amount of filaments attached to the surface of the internal homogenous layer.

Figure 11. Gamonts with gametes and young sporocysts after the fertilization **(A-C).** Abbreviations: amylopectin granule (am), axoneme (Ax), gametocyst wall (CW), dense granule (DG), dense layer (dl), filamentous layer (fl), mitochondrion (M), nucleus (N), sporocyst wall (SW). **A.** Gametocyst wall after the formation of the gametes exhibits a third layer with more dense material under the two layers observed in more early gamont stages (Figure 12). Residual amylopectin and dense granules are observed between the gametes and the gametocyst wall. **B.** Cross sections of flagellar axonemes indicate a male gamete (B) and two serial sections are of a 9+0 pattern. **C.** After the fertilization process the young sporocysts are surrounded by a thin wall covered by very small spines.

Figure 12. Maximum Likelihood (ML) tree inferred on an alignment of 115 small subunit (SSU) rDNA sequences corresponding to 9 *Selenidium* and *Lecudina* species from this current study (highlighted in grey boxes) and 106 sequences from diverse eukaryotes corresponding mostly to representatives of Alveolata with one Rhizaria as outgroup. The Maximum Likelihood method is based on the General Time Reversible +G +I model (Nei and Kumar 2000). The tree is drawn to scale, with branch lengths measured in the number of substitutions per site. A branch was shortened by a multiple (3) of the length of substitutions/site scale bar. There were a total of 1153 positions in the final dataset. ML evolutionary analyses were conducted in MEGA6 (Tamura et al. 2013). Numbers at the branches denote ML bootstrap percentage (first value). Bayesian posterior probabilities are also indicated (second value). Black dots on branches denote bootstrap percentages above 99% and Bayesian posterior probabilities superior to 0.97.

Figure 13. Molecular phylogenetic analysis by Maximum Likelihood method of Selenidiidae lineage retrieved from polychaete annelids (host families in bold black).

The evolutionary history was inferred by using the Maximum Likelihood method based on the General Time Reversible model (Nei and Kumar 2000). The tree with the highest log likelihood (-5446.5092) is shown. A discrete Gamma distribution was used to model evolutionary rate differences among sites (5 categories with gamma parameter = 0.2711). The rate variation model allowed for some sites to be evolutionarily invariable (+I), 39.8364% sites). The tree is drawn to scale, with branch lengths measured in the number of substitutions per site. Novel sequences are highlighted in grey boxes.

Table 1. List of the SSU rDNA sequence numbers of archigregarines and *Veloxidium* initially included in this group and the references: 1. This work; 2. Leander et al. 2003; 3. Leander et al. 2007; 4. Rueckert and Leander 2009; 5. Wakeman and Leander 2012; 6. Wakeman and Leander 2013; 7. Wakeman et al. 2014.

Archigregarines	SSU rDNA sequences	Ref.	Host	Infraclass	Order	Family
Selenidium pendula LG	LN901443	1	*Scolelepis squamata*	Canalipalpata	Spionida	Spionidae
Selenidium pendula IF	LN901444	1	*Scolelepis squamata*	Canalipalpata	Spionida	Spionidae
Selenidium boccardiella	JN857969	5	*Boccardiella ligerica*	Canalipalpata	Spionida	Spionidae
Selenidium mesnili	JN857968	5	*Myxicola infundibulum*	Canalipalpata	Sabellida	Sabellidae
Selenidium hollandei	LN901445	1	*Sabellaria alveolata*	Canalipalpata	Sabellida	Sabellariidae
Selenidium neosabellariae	KC110871 KC110872 KC110873	6	*Neosabellaria cementarium*	Canalipalpata	Sabellida	Sabellariidae
Selenidium identhyrsae	JN857967	6	*Idanthyrsus saxicavus*	Canalipalpata	Sabellida	Sabellariidae
Selenidium serpulae	DQ683562	3	*Serpula vermicularis*	Canalipalpata	Sabellida	Serpulidae
Selenidium sensimae	KC110869 KC110870	6	*Spirobranchus giganteus*	Canalipalpata	Sabellida	Serpulidae
Selenidium Sp1	KC110863 KC110866 KC110867	6	*Spirobranchus giganteus*	Canalipalpata	Sabellida	Serpulidae
Selenidium Sp2	KC110864 KC110865 KC110868	6	*Spirobranchus giganteus*	Canalipalpata	Sabellida	Serpulidae
Selenidium terebellae	AY196709	2	*Thelepus* sp,	Canalipalpata	Terebellida	Theleponidae
Selenidium terebellae	KC890803 KC890804 KC890805 KC890806	7	*Thelepus japonica*	Canalipalpata	Terebellida	Theleponidae
Selenidium melongena	KC890799 KC890800 KC890801 KC890802	7	*Thelepus japonica*	Canalipalpata	Terebellida	Terebellinae
Selenidium cf echinatum	KC110874 KC110875	6	*Dodecaceria concarum*	Canalipalpata	Terebellida	Cirratulidae
Selenidium vivax	AF236097	2	*Phascolosoma agassizii*	Sipunculida	Phascolosimida	Phascolosomatidae
Platyproteum vivax	AY196708	4	*Phascolosoma agassizii*	Sipunculida	Phascolosimida	Phascolosomatidae
Filipodium phascolosoma	FJ832163	4	*Phascolosoma agassizii*	Sipunculida	Phascolosimida	Phascolosomatidae
Selenidium pisinnus	FJ832162	4	*Phascolosoma agassizii*	Sipunculida	Phascolosimida	Phascolosomatidae
Selenidium orientale	FJ832131	4	*Themiste pyroidea*	Sipunculida	Golfingiida	*Veloxidium leptosynaptae*
Veloxidium leptosynaptae	JN857966	5	*Leptosynapta clarki*	Echinodermata	Apodida	Synaptidae

1204 **Table 2**. Summary of biological, geographical and molecular data, for original isolates in
1205 this study. The number of corresponding stages used for DNA preparations is indicated; T,
1206 trophozoite; C, cyst. Gene Accession numbers of the new sequences are available from the
1207 EMBL database.
1208

Gregarine	Host	Location	Isolate names	Stage	Gene Access number (18S)
Selenidium pendula Giard 1884	*Scolelepis squamata (*O. F. Müller 1806)	English Channel, Roscoff, Aber, Lat:48°43'35.25"N, Long:3°59'22.54"W.	*Selenidium pendula* LG	50-70 T	LN901443
Selenidium pendula Giard 1884	*Scolelepis squamata (*O. F. Müller 1806)	English Channel, Roscoff-Aber 2012, Lat:48°43'35.25"N, Long:3°59'22.54"W.	*Selenidium pendula* IF	50-70 T	LN901444
Selenidium hollandei Vivier & Schrével 1966	*Sabellaria alveolata* (Linnaeus 1767)	English Channel, Saint-Efflam-Ile Rouge Lat:48°40'57.96"N, Long:3°35'32.52"W.	*Selenidium hollandei* LG	50-70 T	LN901445
Lecudina pellucida (Mingazzini 1891)	*Perinereis cultrifera* (Grübe 1840)	English Channel, Roscoff-Ile de la Souris, Lat:48°43'41.73"N, Long:3°59'22.10"W.	*Lecudina pellucida* LG	50-70 T	LN901442
Lecudina tuzetae Schrével 1963	*Neanthes (Nereis) diversicolor (*O. F. Müller 1776)	English Channel, Roscoff-Penzé 2012, Lat:48°37'40.07"N, Long:3°57'13.40"W.	*Lecudina tuzetae Roscoff 2012* IF132	7 C	LN901446
Lecudina tuzetae Schrével 1963	*Neanthes (Nereis) diversicolor (*O. F. Müller 1776)	English Channel, Roscoff-Penzé 2013, Lat:48°37'40,07"N, Long:3°57'13.40"W.	*Lecudina tuzetae Roscoff 2013a* IF181	30 C	LN901447
Lecudina tuzetae Schrével 1963	*Neanthes (Nereis) diversicolor (*O. F. Müller 1776)	English Channel, Roscoff-Penzé 2013, Lat:48°37'40.07"N, Long:3°57'13.40"W.	*Lecudina tuzetae Roscoff 2013b* IF462	2 C	LN901448
Lecudina tuzetae Schrével 1963	*Neanthes (Nereis) diversicolor (*O. F. Müller 1776)	English Channel, Roscoff-Penzé 2014, Lat:48°37'40,07"N, Long:3°57'13.40"W.	*Lecudina tuzetae Roscoff 2014a* IF171	50 C	LN901449
Lecudina tuzetae Schrével 1963	*Neanthes (Nereis) diversicolor (*O. F. Müller 1776)	English Channel, Roscoff-Penzé 2014, Lat:48°37'40,07"N, Long:3°57'13.40"W.	*Lecudina tuzetae Roscoff 2014b* IF172	50 C	LN901450

1209
1210

Figure 1 tif

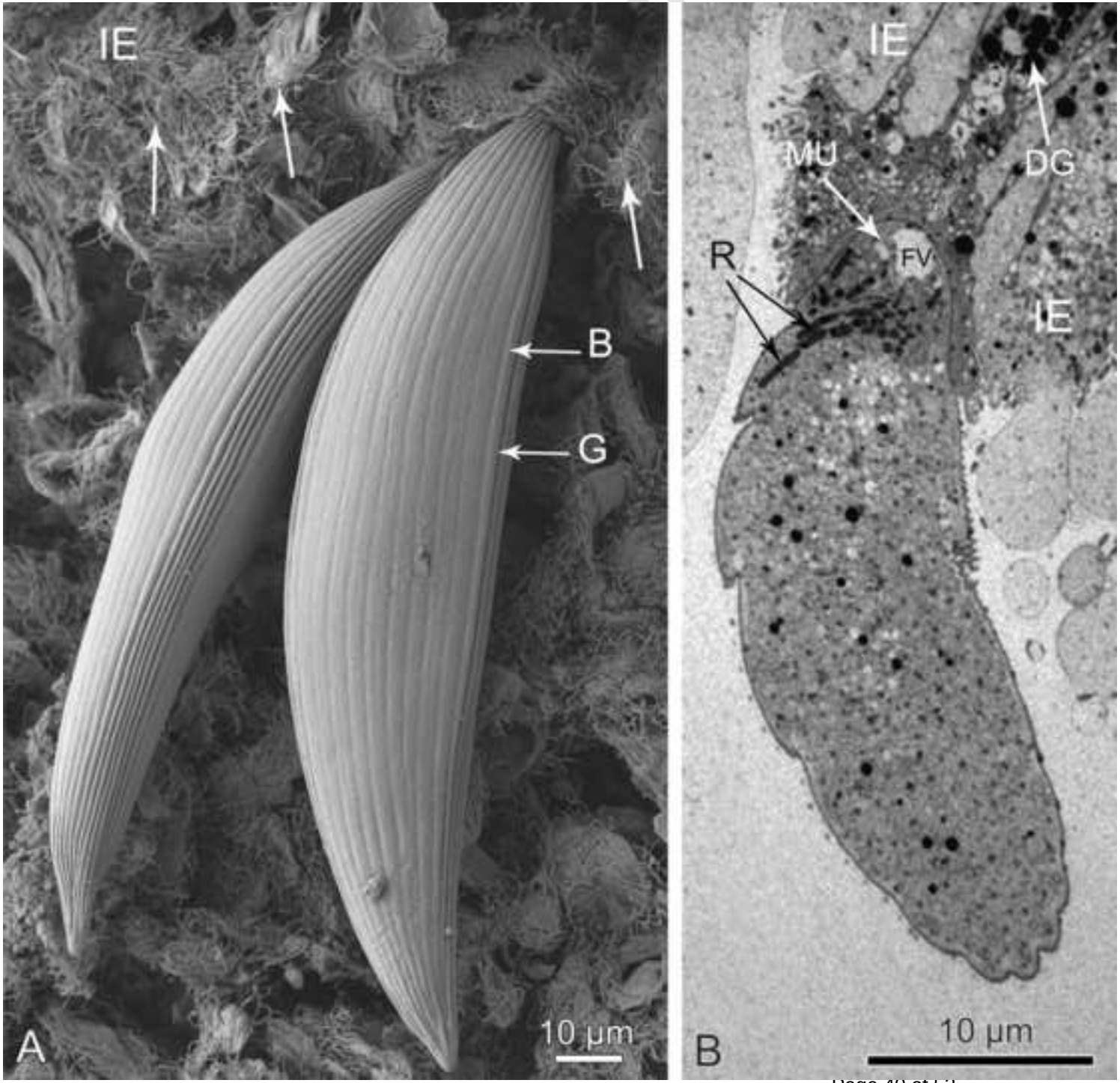

Figure 2 tif

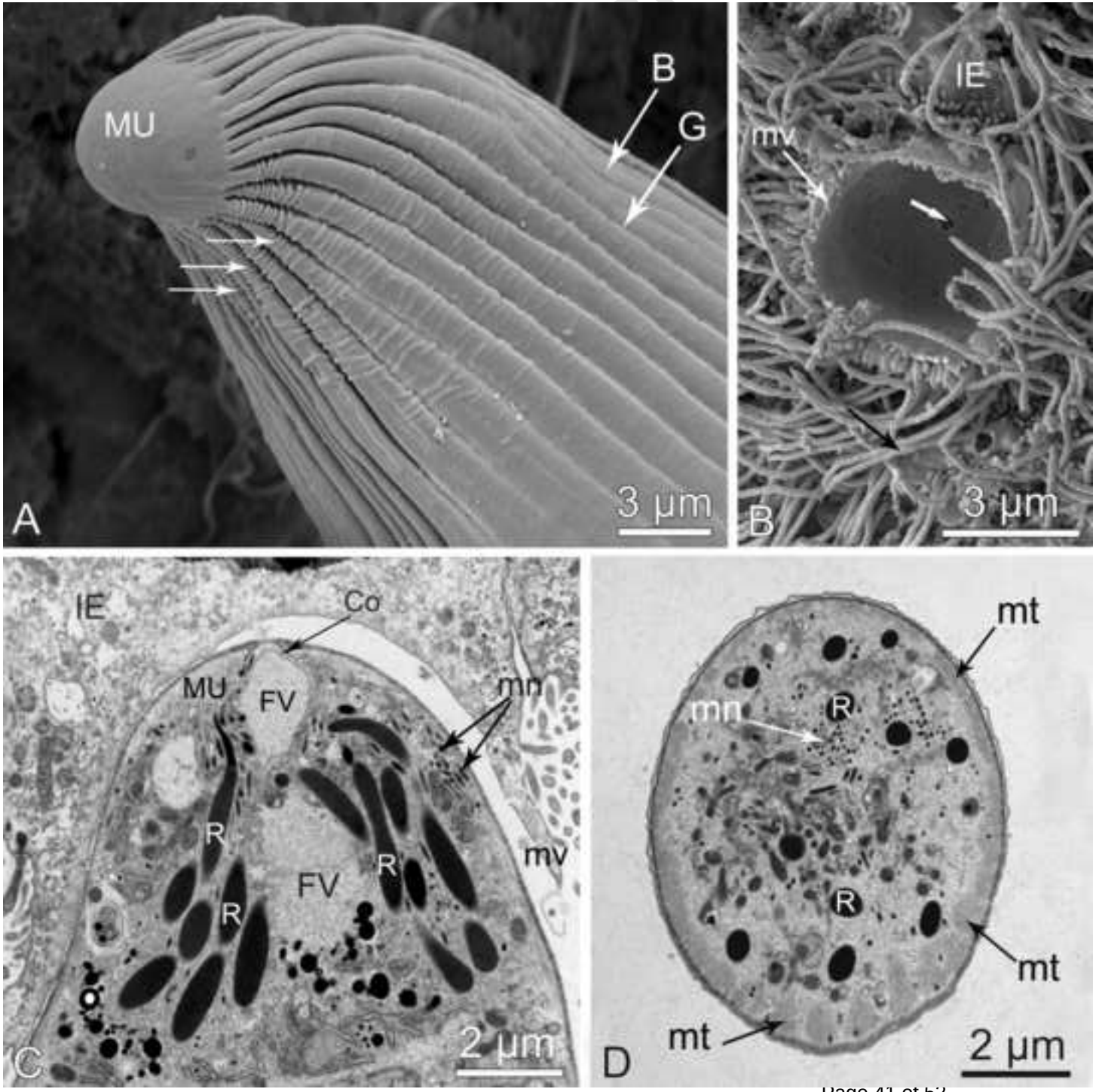
MU
B
G
3 µm
A
IE
mv
3 µm
B
IE
Co
MU
FV
mn
R
R
FV
R
mv
2 µm
C
mt
mn
R
R
mt
mt
2 µm
D

Figure 3 tif

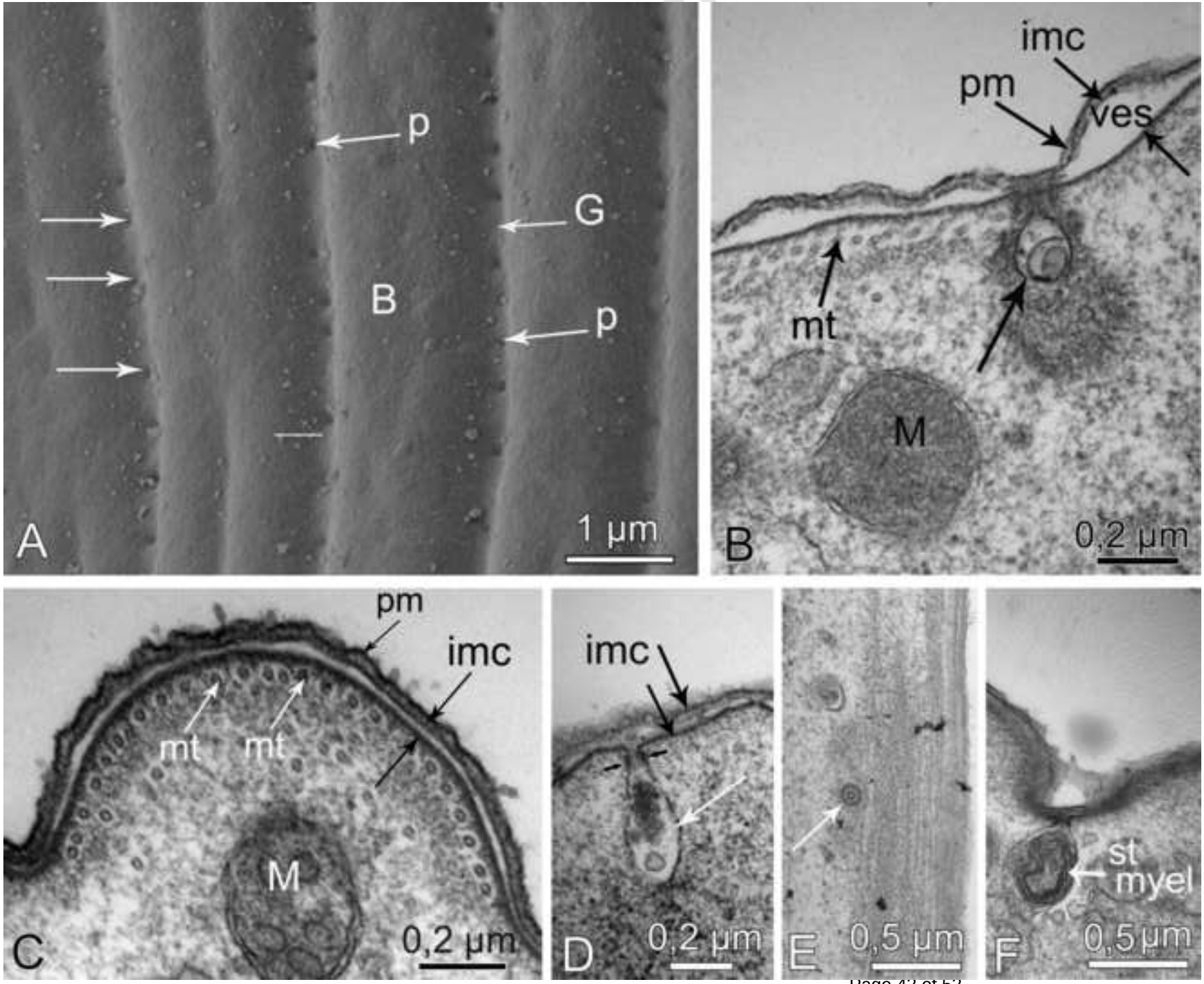
p
G
B
p
1 µm
A
imc
pm
ves
mt
M
0,2 µm
B
pm
imc
mt
mt
M
0,2 µm
C
imc
0,2 µm
D
0,5 µm
E
st
myel
0,5 µm
F

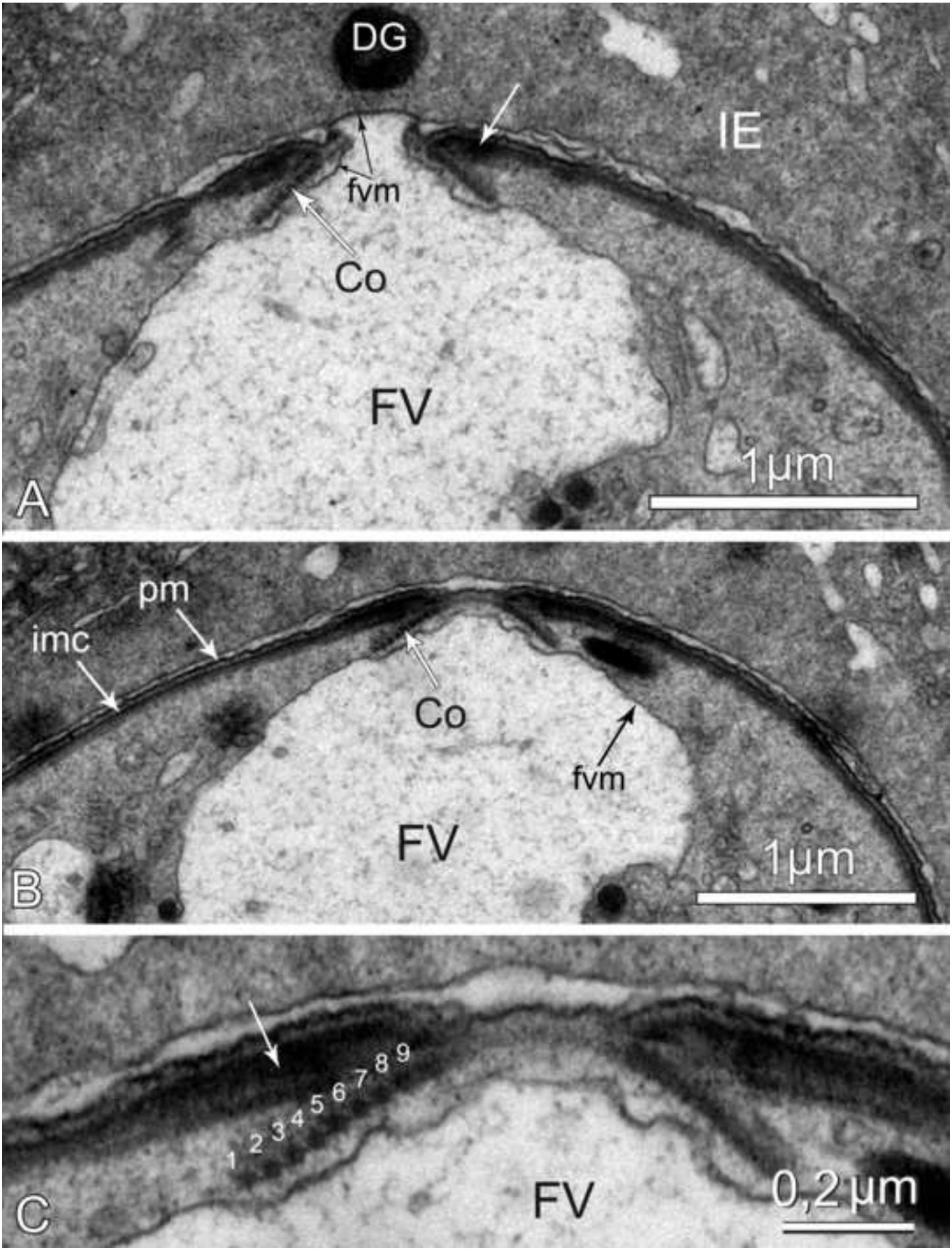

Figure 5 tiff

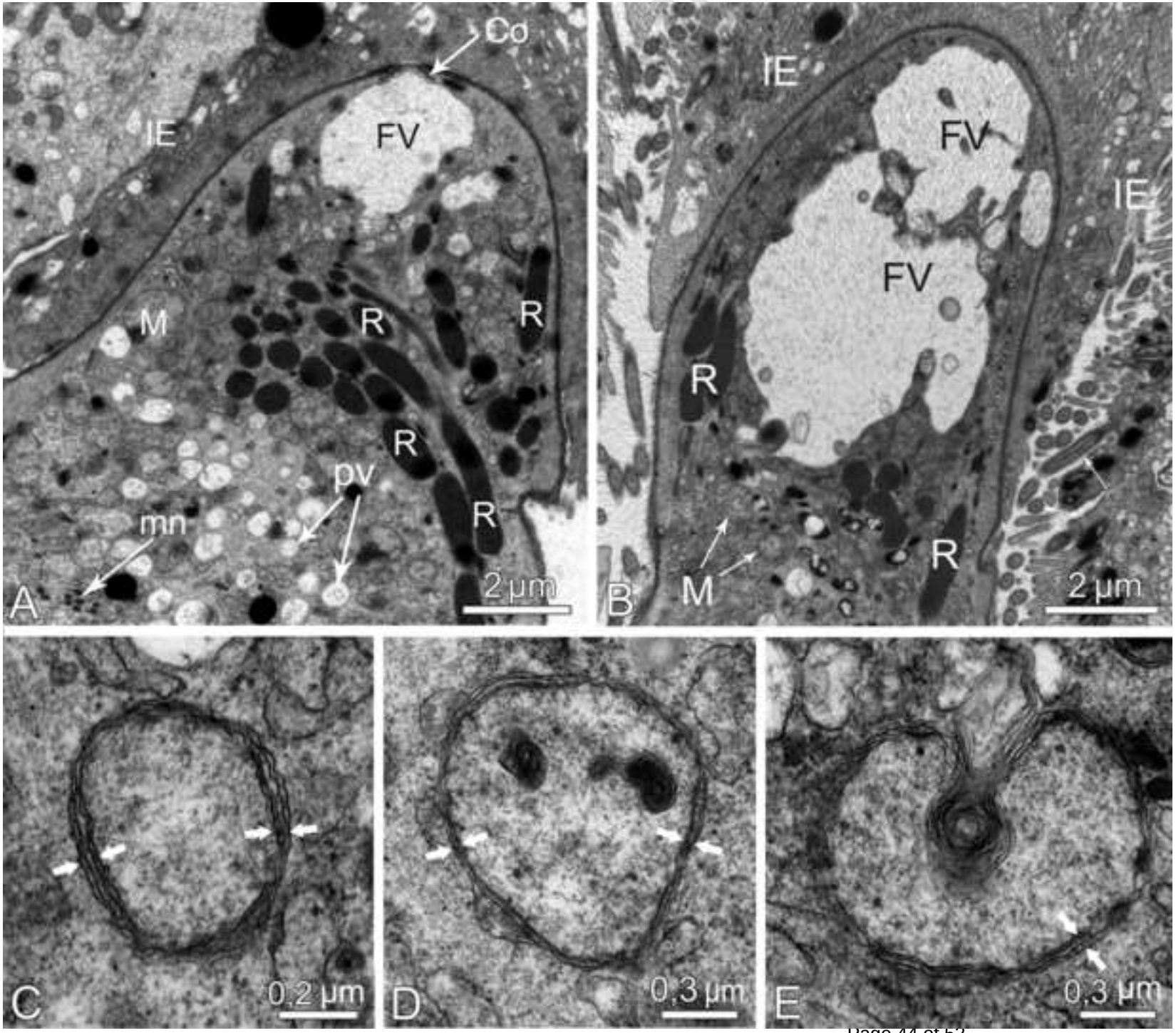

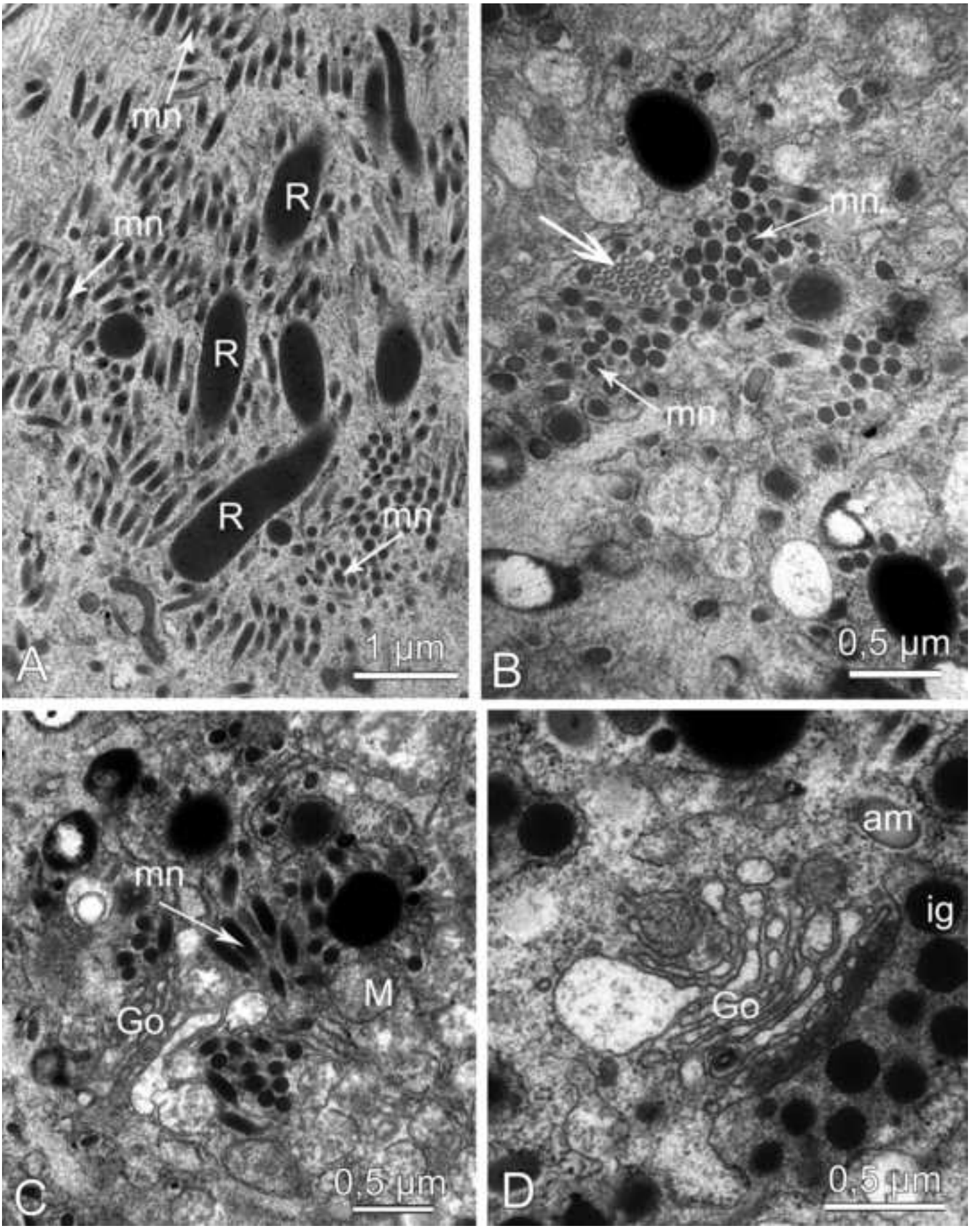

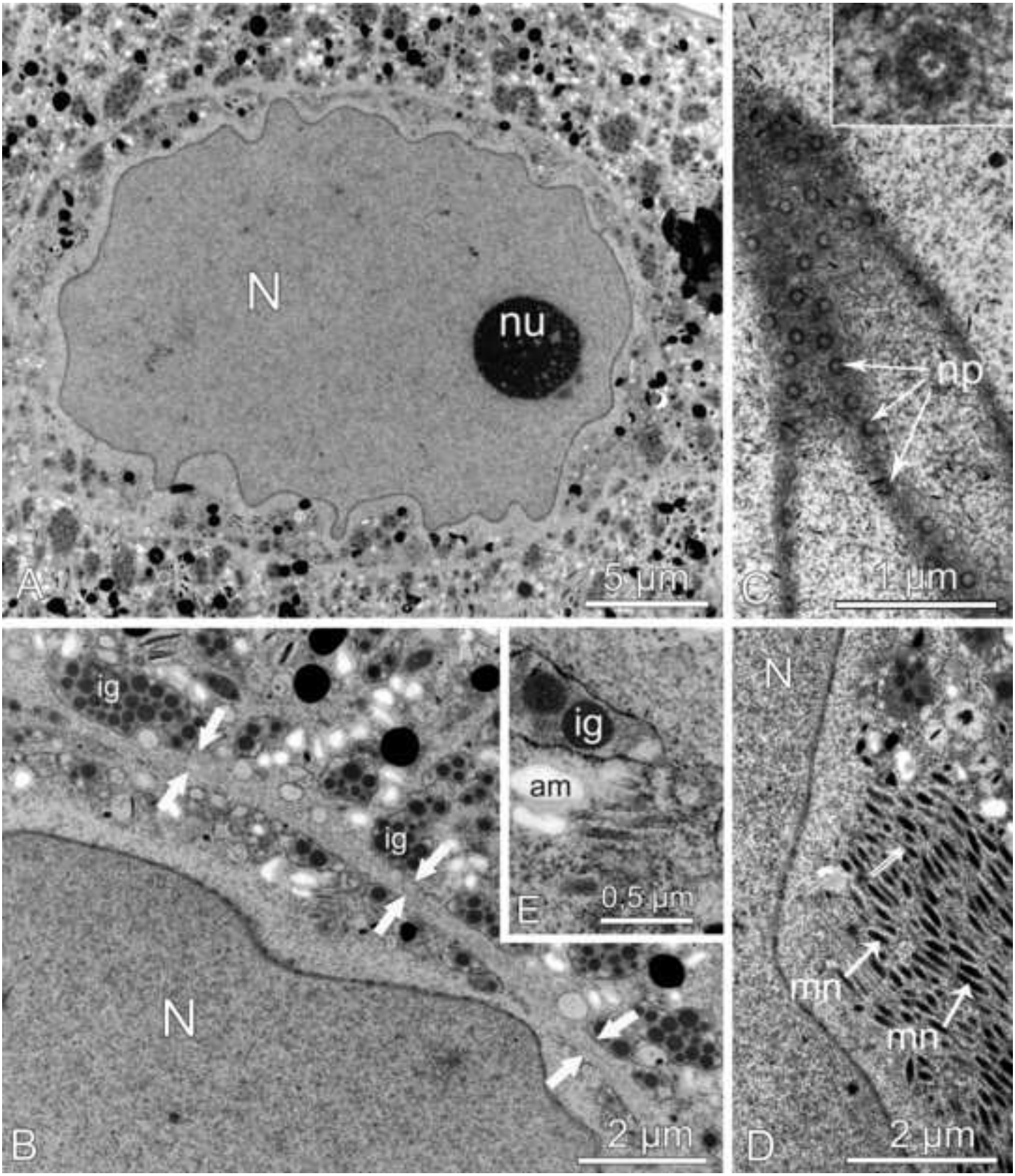

Figure 8 tif

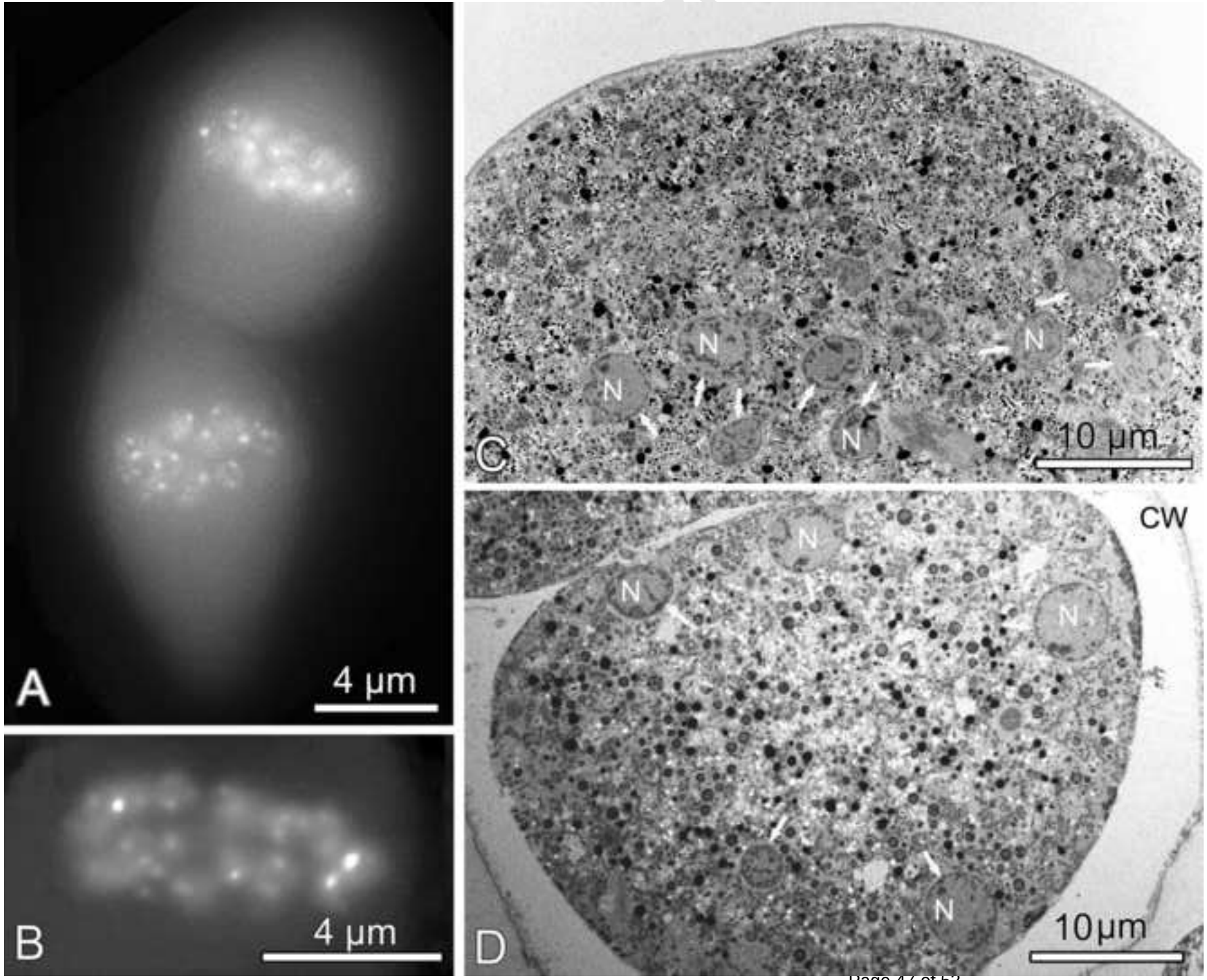

Figure 9 tif

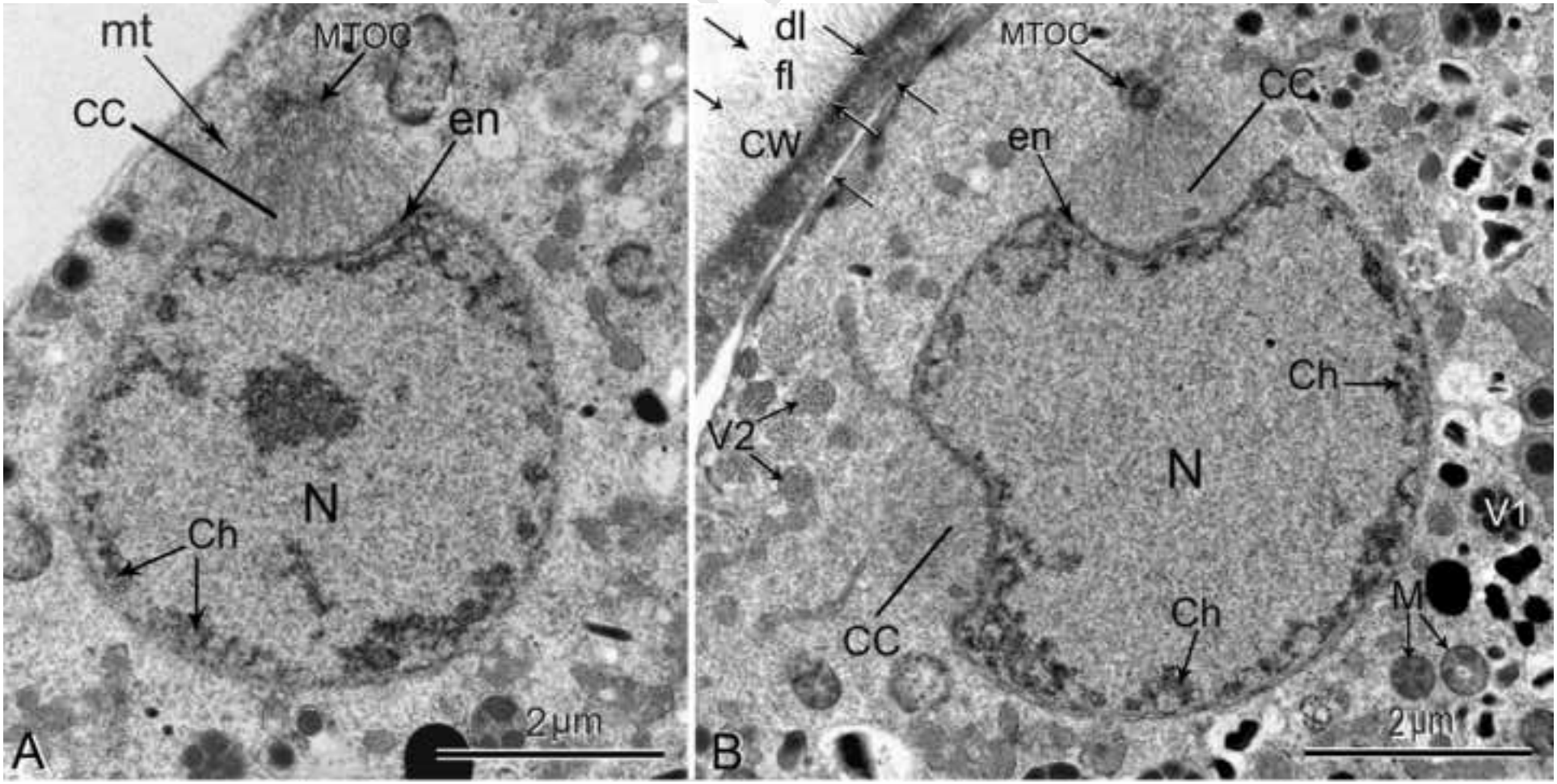

Figure 10 tif